Impact of phytoplankton community size on a linked global ocean optical and ecosystem model

Colleen B. Mouw[*a1], James A. Yoder[a2], and Scott C. Doney[b]

[*]Corresponding author
please use current address[1]

[a]University of Rhode Island
Graduate School of Oceanography
215 South Ferry Road
Narragansett, RI 02882
USA

[b]Woods Hole Oceanographic Institution
266 Woods Hole Road
Woods Hole, MA 02543
USA
sdoney@whoi.edu

[1]now at University of Wisconsin-Madison
Space Science and Engineering Center
1225 West Dayton Street
Madison, WI 53706
USA
Phone/fax: +1 608-263-1787
colleen.mouw@ssec.wisc.edu

[2]now at Woods Hole Oceanographic Institution
266 Woods Hole Road
Woods Hole, MA 02543
USA
jyoder@whoi.edu

Published in *Journal of Marine Systems* (2012) 89: 61-75.

Abstract

We isolated the effect phytoplankton cell size has on varying remote sensing reflectance spectra ($R_{rs}(\lambda)$) in the presence of optically active constituents by using optical and radiative transfer models linked in an offline diagnostic calculation to a global biogeochemical/ecosystem/circulation model with explicit phytoplankton size classes. Two case studies were carried out, each with several scenarios to isolate the effects of chlorophyll concentration, phytoplankton cell size, and size-varying phytoplankton absorption on $R_{rs}(\lambda)$. The goal of the study was to determine the relative contribution of phytoplankton cell size and chlorophyll to overall $R_{rs}(\lambda)$ and to understand where a standard band ratio algorithm (OC4) may under/overestimate chlorophyll due to $R_{rs}(\lambda)$ being significantly affected by phytoplankton size. Phytoplankton cell size was found to contribute secondarily to $R_{rs}(\lambda)$ variability and to amplify or dampen the seasonal cycle in $R_{rs}(\lambda)$, driven by chlorophyll. Size and chlorophyll were found to change in phase at low to mid-latitudes, but were anti-correlated or poorly correlated at high latitudes. Phytoplankton size effects increased model calculated $R_{rs}(443)$ in the subtropical ocean during local spring through early fall months in both hemispheres and decreased $R_{rs}(443)$ in the Northern Hemisphere high latitude regions during local summer to fall months. This study attempts to tease apart when/where variability about the OC4 relationship may be associated with cell size variability. The OC4 algorithm may underestimate [Chl] when the fraction of microplankton is elevated, which occurs in the model simulations during local spring/summer months at high latitudes in both hemispheres.

Keywords: phytoplankton cell size; chlorophyll; remote sensing reflectance; ecosystem modeling; optics; global ocean

1. Introduction

Biogeochemical/ecosystem/circulation models represent our best estimate of global distributions of many biogeochemical parameters at temporal and spatial scales unattainable by ship-based observations and/or unobservable from satellite platforms. They play an important role in our understanding of how ocean biogeochemistry and carbon cycling operates as an integrated ecological, physical and chemical system. These models are crucial for understanding observed trends in satellite observations (Antoine et al., 2005; Gregg et al., 2005); can help inform satellite-based primary production algorithms that strive to incorporate ecological information beyond just chlorophyll concentration (Mouw and Yoder, 2005); can be used to link observed variability in bloom functioning to variability in carbon export and air-sea CO_2 fluxes (Bennington et al., 2009); and are the basis for predictions about the future state of marine ecology, biogeochemistry, and ocean carbon storage in a changing climate (Bopp et al., 2001; Orr et al., 2005; Henson et al. 2010).

A significant amount of research has gone into linking observed biogeochemical variables to optical properties (Dickey et al., 2006). Progress in ocean color remote sensing technology and inversion algorithms has provided ways to assess standing stocks of phytoplankton pigments (Maritorena et al., 2002; O'Reilly et al., 1998), carbon (Behrenfeld et al., 2005), particulate organic carbon (Stramski et al., 1999), colored dissolved and detrital material (CDM) (Maritorena et al., 2002), and most recently phytoplankton size structure (Mouw and Yoder, 2010; Bracher et al. 2009; Kostadinov et al., 2009; Hirata et al., 2008; Ciotti and Bricaud 2006; Uitz et al. 2006). Given the progress in optical observational capabilities, if we are to compare models to measurements and/or assimilate measurements into models, it is necessary to model not only the biogeochemical, but also the optical properties as state variables,

and to directly compare model results to remotely sensed and *in situ* measurements (Fujii et al., 2007; Gregg and Casey, 2009).

Physical and biogeochemical processes drive the distribution of optical properties in the ocean, and the study of upper ocean ecology requires a clear understanding of optics. One can argue that these fields are intricately linked and the future developments in either of these fields will require integrated approaches to both of their studies (Bissett et al., 2001). Yet, there have been only a few attempts to link optics to ecosystem models. The coupled physical-ecosystem-optical models that have been developed thus far (Bissett et al., 1999a; Bissett et al., 1999b; Fujii et al., 2007; Gregg and Casey, 2009) have demonstrated a better fit with observations and were able to more closely reproduce biogeochemical processes than their non-optical counterparts. Beyond these few exceptions, most ecosystem models use sophisticated treatments of physical mixing, circulation and biology but use oversimplified physics and bio-optics associated with the underwater light field. It has been recommended that ecosystem models be developed to include optics (Rothstein et al., 2006), while others (Liu et al., 1999) have indicated that the empirical simplistic optical models used to parameterize scalar irradiance or photosynthetically available radiation in terms of chlorophyll concentration (Morel, 1988) are insufficient in comparison to numerical radiative transfer software such as Hydrolight (Mobley, 1989; Mobley and Sundman, 2008a; Mobley and Sundman, 2008b).

We focus our efforts on understanding the impact of considering phytoplankton cell size within optical constructs. Phytoplankton cell size is important ecologically in determining both the intensity and efficiency of carbon fixation and export. Cell size is also important optically. There are notable differences in the absorption of pico (< 2 μm) (Ciotti and Bricaud, 2006) and micro (> 20 μm) phytoplankton cells (Ciotti et al., 2002). The absorption spectra of a given

phytoplankton size class change with intracellular chlorophyll concentration (packaging effect) (Duysens, 1956). Microphytoplankton cells have a lower specific absorption coefficient and dampened peak absorption heights relative to their troughs compared to picophytoplankton (Bricaud et al., 1983). Kostadinov et al. (2009; 2010) has demonstrated success retrieving phytoplankton cell size distribution from satellite measurements, based on relationships between the backscattering slope and the slope of the particle size distribution. Mouw and Yoder (2010) also demonstrated successful retrieval of phytoplankton cell size distribution based on absorption relationships. Given the demonstrated success with an absorption-based approach, this study focused on absorption as the primary characterization of optical difference in phytoplankton. Several scenarios were evaluated to isolate phytoplankton cell size and chlorophyll concentration compared to full variability of the model.

In this study, we apply optical and radiative transfer models (Mobley 1989; Mobley and Sundman 2008a; Mobley and Sundman 2008b) to the output of a global biogeochemical / ecosystem / circulation model (Doney et al., 2009). The linking of the optical and radiative transfer models were performed as an off-line diagnostic, having no feedback with the ecosystem / biogeochemical model (Fig. 1). For our application, model output was used to provide a reasonable approximation of the time-space variability and co-variability of phytoplankton chlorophyll, colored dissolved organic matter and phytoplankton cell size in the global ocean. The purpose was to allow for a clear understanding of the role various optical parameters play in the overall remote sensing reflectance spectra ($R_{rs}(\lambda)$, sr^{-1}).

$R_{rs}(\lambda)$ is a measure of the proportion of the downwelling light incident onto the water surface that is eventually returned through the surface at a direction detected by a radiometer (Mobley, 1994). $R_{rs}(\lambda)$ is the primary parameter derived from satellite ocean color radiometer

measurements (after calibration and atmospheric correction) and thus has the least amount of associated uncertainty compared to secondary derived products such as chlorophyll concentration. For example, SeaWiFS R_{rs} accuracy is 9-12% over the majority of the ocean, while the uncertainty associated with the NASA standard chlorophyll algorithm (ocean color 4-band ratio, OC4) (O'Reilly et al. 1998) is on average 35% (Bailey and Werdell, 2006). In addition to greater uncertainty in derived chlorophyll estimates, there are numerous approaches to estimate chlorophyll concentration from satellite remote sensing that range from empirical band ratios (O'Reilly et al. 1998 and references therein) to semi-analytical inversions (Carder et al. 1999; Maritorena et al. 2002; Doerffer and Schiller, 2007). All chlorophyll retrieval approaches ultimately utilize $R_{rs}(\lambda)$. To best inform the many possible chlorophyll retrieval approaches, the emphasis of this paper is on the impact phytoplankton cell size has on $R_{rs}(\lambda)$. To put the cell size impact into a more familiar context, we also demonstrate the impact size has on chlorophyll estimated from the NASA standard chlorophyll algorithm. The specific objectives of this study are to 1) *determine relative contribution of chlorophyll concentration and phytoplankton cell size variation to overall $R_{rs}(\lambda)$ variation and 2) understand where standard algorithms will under/over estimate chlorophyll concentration due to $R_{rs}(\lambda)$ being significantly affected by phytoplankton size.*

2. Methods

2.1 Biogeochemistry/ecosystem/circulation model

We used the Community Climate System Model (CCSM-3) coupled ocean Biogeochemical Elemental Cycling (BEC) model (Doney et al., 2009). The BEC model consists of upper ocean ecological (Moore et al., 2002b; Moore et al., 2004) and full-depth

biogeochemical (Doney et al., 2006) modules embedded in a global three dimensional Parallel Ocean Program (POP) ocean general circulation model (Collins et al., 2006; Smith and Gent 2004). The ecological component includes multiple nutrients and phytoplankton functional groups; the coupled biogeochemical model incorporates carbon, oxygen, nitrogen, phosphorus, silicon, and iron dynamics. The model is forced with physical climate forcing from atmospheric reanalysis and satellite data products (Doney et al., 2007) and time varying dust deposition (Mahowald et al., 2003).

There are fourteen main model components: three phytoplankton classes, zooplankton, suspended/dissolved detritus and sinking particulate detritus, dissolved nitrate, ammonia, phosphorus, iron, silicate, oxygen, dissolved inorganic carbon, and alkalinity. The three model phytoplankton compartments include a small fraction consisting of pico/nanoplankton (< 20 μm), diatoms (considered to be all microplankton, > 20 μm) and diazotrophs. The pico/nanoplankton size class is designed to replicate the rapid and highly efficient nutrient recycling found in many subtropical, oligotrophic environments. Diatoms in the model are a larger, bloom-forming size class. As described later in section 2.2.2, diazotroph phytoplankton (generally considered to be *Trichodesmium* spp.) are not assigned to a size class because of their unique absorption and scattering properties. Instead, they are considered a separate class and do not contribute to the phytoplankton size effects investigated in this study. Phytoplankton growth rates are determined by available light and nutrients (Geider et al., 1998). Photoadaption is parameterized with dynamically adaptive chlorophyll/carbon ratios. The diazotrophs fix all nitrogen from N_2 gas, and calcification is parameterized as a fraction of the pico/nanoplankton production as a function of temperature and nutrients adapted for coccolithophores (Doney et al., 2009). The model has one adaptive zooplankton class that grazes on phytoplankton and sinking

detritus. Size structure effects are included by varying key zooplankton parameters depending on the food source (Lima and Doney, 2004). A single zooplankton pool grazes on all phytoplankton groups. Zooplankton parameters for grazing and routing of material among remineralization and detrital pools vary depending on the type of prey being consumed. Consistent with field observations, when zooplankton diets are dominated by diatoms zooplankton grazing rates lower and more material from zooplankton grazing and mortality is routed to sinking detritus. This grazing pattern reflects generally larger predators (e.g., copepods) and sinking fecal pellet production. The model suspended/dissolved detrital pool is equivalent to the semi-labile component of dissolved organic matter (DOM) and is remineralized with a life-time of several months. The model does not explicitly treat the refractory component of DOM.

2.2 Optical model

An optical model was linked to the CCSM-3 BEC model output in an offline diagnostic calculation performed on each grid cell (resolution of 3.6° in longitude, 0.8° to 1.8° in latitude). The CCSM-3 BEC model output used in the optical model included size fractionated chlorophyll concentration (pico-/nanoplankton and diatoms only), *Trichodesmium* spp. chlorophyll concentration (diazotrophs) and dissolved organic carbon (DOC) (Fig. 1). We worked with CCSM-3 BEC global monthly output for 2004, the most recent year of the model simulations available at the time the study was initiated. The model grid has an unevenly spaced vertical distribution across twenty-four layers, with higher resolution in the surface ocean. We averaged the model output over the first photic depth ($1/K_d$). The attenuation coefficient (K_d) was determined from the linear regression of the log of the modeled photosynthetically active

radiation (PAR) versus depth (z). The ecosystem state variables were converted to inherent optical properties (IOPs; absorption and scattering). The IOPs were then converted to apparent optical properties (AOPs), specifically $R_{rs}(\lambda)$, through the radiative transfer software Hydrolight, version 5 (Mobley, 1994; Mobley and Sundman, 2008a; Mobley and Sundman, 2008b) (Fig. 2).

Total absorption is the summation of absorption due to seawater (a_w, m^{-1}) (Pope and Fry, 1997), size-dependent phytoplankton absorption (a_{size}, m^{-1}) (Ciotti et al., 2002; Ciotti and Bricaud, 2006), *Trichodesmium* spp. absorption (Subramaniam et al., 1999b) and the absorption due to CDM (a_{CDM}, m^{-1}) (Bissett et al., 1999a; Bissett et al., 2004). Total scattering is the summation of seawater scattering (b_w, m^{-1}) (Morel, 1974), size dependent (b_{size}, m^{-1}) scattering (Morel and Maritorena, 2001), and *Trichodesmium* spp. scattering (Subramaniam et al., 1999a) (Figs. 2 and 3):

$$a(\lambda) = a_w(\lambda) + a_{size}(\lambda) + a_{tri}(\lambda) + a_{CDM}(\lambda) \quad (1)$$

$$b(\lambda) = b_w(\lambda) + b_{size}(\lambda) + b_{tri}(\lambda) \quad (2)$$

A description of the absorption and scattering properties for each of the non-water components follows. A summary of the parameter notation can be found in Table 1.

2.2.1 Size Fractionated Phytoplankton

For the phytoplankton size considerations, total size dependent chlorophyll ($[Chl_{size}]$, mg m^{-3}) (Fig. 4a) was calculated as,

$$[Chl_{size}] = [Chl_{micro}] + [Chl_{small}] \quad (3)$$

where $[Chl_{micro}]$ and $[Chl_{small}]$ (unit: mg m^{-3}) are the CCSM-3 BEC model output for the microplankton and the combined pico- and nanoplankton size fractionated chlorophyll concentration, respectively. The phytoplankton size parameter (S_f, %) was first introduced by Ciotti et al. (2002) to represent the percentage of picoplankton in a community. Similar to Mouw and Yoder (2005; 2010) and due to the combination of the pico- and nanoplankton size

classes in the CCSM-3 BEC model, we utilized a different size parameter defined as the percentage of microplankton in a community (S_{fm}) (Fig. 4b). S_{fm} is given by $S_{fm}=1-S_f$ and varies from 0%, where a phytoplankton assemblage is dominated by picoplankton, to 100% where it is dominated by microplankton. The percentage of microplankton in a phytoplankton community was calculated as

$$S_{fm} = [Chl_{micro}]/([Chl_{small}] + [Chl_{micro}]) \quad (4)$$

Ciotti et al. (2002) demonstrated that despite taxonomic and physiological variability in phytoplankton community structure, variation in the spectral shape of the chlorophyll-specific absorption coefficient could be described by an abundance-weighted average of absorption spectra for micro- and picoplankton (Fig. 3). Therefore, the size-dependent chlorophyll-specific absorption of phytoplankton ($a^*_{size}(\lambda)$, $m^2\ mg^{-1}$) was represented as a spectral mixing model (Ciotti et al., 2002)

$$a^*_{size}(\lambda) = [(S_f)\ a^*_{pico}(\lambda)] + [(1-S_f)\ a^*_{micro}(\lambda)] \quad (5)$$

where spectral chlorophyll-specific absorption due to picoplankton ($a^*_{pico}(\lambda)$, $m^2\ mg^{-1}$) (Ciotti and Bricaud, 2006) and microplankton ($a^*_{micro}(\lambda)$, $m^2\ mg^{-1}$) (Ciotti et al., 2002) were prescribed, percent picoplankton (S_f, varies between 0 and 100%) weights the spectra between the size extremes, and $S_{fm}=1-S_f$. The spectral size dependent phytoplankton absorption coefficient $a_{size}(\lambda)$ (m^{-1}) was derived by multiplying the size-dependent chlorophyll concentration ([Chl_{size}], mg m^{-3}) by the chlorophyll-specific, size weighted absorption ($a^*_{size}(\lambda)$, $m^2\ mg^{-1}$)

$$a_{size}(\lambda) = [Chl_{size}]\ a^*_{size}(\lambda) \quad (6)$$

The size dependent backscattering due to particles ($b_{b\ size}$, m^{-1}) was modeled in the same manner as Morel and Maritorena (2001, their equations 13 and 14), using only the size-dependent chlorophyll concentration (mg m^{-3})

$$b_{b\,size}(\lambda) = 0.416\,[Chl_{size}]^{0.766}\,[0.002 + 0.01(0.5\text{-}0.25\,\log_{10}[Chl_{size}])\,(\lambda/550)^{\nu}] \quad (7)$$

where the exponent ν allows for altering the backscattering relationship associated with particle size as a function of chlorophyll concentration (Morel and Maritorena, 2001).

$$\nu = 0.5(\log_{10}[Chl_{size}]\text{-}0.3) \quad \text{for } 0.02 \text{ mg m}^{-3} < [Chl_{size}] < 2 \text{ mg m}^{-3} \quad (8a)$$

$$\nu = -1.1495 \quad \text{for } [Chl_{size}] \leq 0.02 \text{ mg m}^{-3} \quad (8b)$$

$$\nu = 0 \quad \text{for } [Chl_{size}] \geq 2 \text{ mg m}^{-3} \quad (8c)$$

Spectral backscattering is the proportion of total light that is scattered in the backward direction from a beam. Total scattering is the summation of scattering in both the forward and backward directions. Spectral backscattering was converted to total scattering ($b(\lambda)$) with the backscattering efficiency (B_{size}, 1%) as in Morel and Maritorena (2001).

$$b_{size}(\lambda) = b_{bsize}(\lambda)/B_{size} \quad (9)$$

2.2.2 Diazotroph Phytoplankton

The CCSM-3 BEC model contains information specific to diazotroph biomass and chlorophyll concentration. The absorption and scattering characteristics of *Trichodesmium* spp. are much different than most other phytoplankton species (Fig. 3). Their unique optical properties do not follow those associated with changes in cell size, and require that they be modeled optically as a separate constituent (Fig. 2). As with size dependent phytoplankton, the spectral *Trichodesmium* spp. absorption coefficient was calculated by multiplying the chlorophyll concentration due to *Trichodesmium* spp. ($[Chl_{tri}]$, mg m^{-3}) by the chlorophyll-specific size weighted absorption for *Trichodesmium* spp. ($a^*_{tri}(\lambda)$, m^2 mg^{-1}) (Westberry et al., 2005)

$$a_{tri}(\lambda) = [Chl_{tri}]\, a^*_{tri}(\lambda) \quad (10)$$

where $a^*_{tri}(\lambda)$ was measured by the quantitative filter technique (Subramaniam et al., 1999b), and $[Chl_{tri}]$ was output from the CCSM-3 BEC model.

The spectral backscattering due to *Trichodesmium* spp. ($b_{b\,tri}(\lambda)$), was calculated by multiplying the chlorophyll concentration due to *Trichodesmium* spp. ($[Chl_{tri}]$, mg m^{-3}) by the chlorophyll-specific backscattering for *Trichodesmium* spp. ($b^*_{b\,tri}(\lambda)$, m^2 mg^{-1}) (Westberry et al., 2005)

$$b_{btri}(\lambda) = [Chl_{tri}]\, b^*_{btri}(\lambda) \quad (11)$$

where $b^*_{b\,tri}(\lambda)$ was determined *in vitro* (Subramaniam et al., 1999a). Spectral backscattering due to *Trichodesmium* spp. was converted to total scattering ($b_{tri}(\lambda)$) with the backscattering efficiency (B_{tri}) of 0.4% (Subramaniam et al., 1999a).

$$b_{tri} = b_{btri}/B_{tri} \quad (12)$$

2.2.3 Non-phytoplankton Carbon Pool

In order to utilize the non-phytoplankton carbon pool contained within the CCSM-3 BEC model, a few assumptions were applied. Bissett et al. (1999a) describes in detail the justification for assumed values of constants used to convert total DOC to the colored fraction of DOC. While this assumption contradicts the Siegel et al. (2002) observation that basin-scale distributions of CDM and DOC are largely unrelated, the ability to convert from ecosystem state variables to optically active constituents was a necessary step to calculate $R_{rs}(\lambda)$. As will be discussed in detail later, the analysis was based on the difference between scenarios where only a single parameter was varied and all other optically active constituents were treated identically. Thus, the optical treatment of DOC does not impact the results. Bissett et al. (1999a, 2004) utilized separate labile and relict DOC pools. The CCSM-3 BEC model's DOC pool is semi-labile (a background ~45 μmol/kg of refractory DOC would need to be added to match observed DOC levels). Given the CCSM-3 BEC varying DOC pool is semi-labile, we utilized the Bissett et al. (1999a, 2004) constants for the labile DOC pool. To convert the DOC concentration

([DOC], mg C m^{-3}) to the concentration of colored dissolved material ([CDM], mg m^{-3}) a constant 3.23% of the labile [DOC] pool was assigned as colored ($color_{CDM}$, %) (Bissett et al., 1999a; Bissett et al., 2004)

$$[CDM] = color_{CDM}\,[DOC] \quad (13)$$

Additionally, to move from [CDM] to absorption due to CDM ($a_{CDM}(\lambda)$, m^{-1}) the weight-specific absorption at a reference wavelength needed to be applied. Bissett et al. (1999a, 2004) also determined an appropriate conversion factor for a reference wavelength of 410 nm.

$$a_{CDM}(\lambda_o) = a^*_{CDM}(\lambda_o)\,[CDM] \quad (14)$$

where $a^*_{CDM}(\lambda_o)$, is the weight-specific absorption due to labile CDM at 410 nm and is equal to 0.00508 $m^2 mg^{-1}$ (Bissett et al., 1999a; Bissett et al., 2004). The spectral absorption due to CDM can then be calculated as an exponential function

$$a_{CDM}(\lambda) = a_{CDM}(\lambda_0)\exp[-S(\lambda-\lambda_0)] \quad (15)$$

where S is the slope of the exponential relationship and assigned a global average value of 0.015 nm^{-1} (Barnard et al., 1998) (Fig. 3).

2.3 Radiative transfer model

The IOP output from the optical model was passed to Hydrolight 5 (Mobley, 1994; Mobley and Sundman, 2008a; Mobley and Sundman, 2008b), a radiative transfer software, to compute the apparent optical properties (AOP). Hydrolight was run with four optical components including, water, size fractionated phytoplankton, diazotroph phytoplankton and colored dissolved material as described above. Raman scattering, chlorophyll and colored dissolved material fluorescence were included and the water column was assumed to be infinitely deep (no bottom reflectance). A semi-analytical sky model was used with a specified

solar zenith angle of 30°. Aerosol type, wind speed, average sea level pressure, relative humidity, precipitable water content and horizontal visibility were assumed to be marine, 5 m/s, 29.92 inches of Hg, 15%, 4 cm, and 300 km, respectively. The AOP values were computed only at specific band-width intervals equivalent to the wavelength bands observed by SeaWiFS (412, 443, 490, 510, 555, and 670 nm). The AOP of particular interest was $R_{rs}(\lambda)$ because it is the parameter directly derived from satellite radiometer measurements (after calibration and atmospheric correction have been applied). The optical model as described above, applied to each grid cell of the CCSM-3 BEC model output, was used to capture the full variability in $R_{rs}(\lambda)$ associated with varying chlorophyll concentration, phytoplankton size assemblage and size –varying phytoplankton absorption.

2.4 Optical Scenarios

In an effort to isolate the effects of chlorophyll concentration, phytoplankton cell size and size-varying phytoplankton absorption on overall $R_{rs}(\lambda)$ we performed two case studies each with several different scenarios. The goals of the two case studies were different. The first case study was used to understand the relative contribution of phytoplankton cell size and chlorophyll concentration variation to overall $R_{rs}(\lambda)$ variation. In this case study, the CCSM-3 BEC model output was averaged over all months for 2004. With the annual average model output we ran the following scenarios, 1) full cell size and chlorophyll concentration variability, 2) chlorophyll concentration held constant at the global mean (0.17 mg m^{-3}) and, 3) phytoplankton size composition held constant at the global mean (35% microplankton) (Fig. 4). These scenarios allowed us to independently quantify the impact variation in chlorophyll alone and phytoplankton size alone impart on $R_{rs}(\lambda)$ variation. It is believed that chlorophyll variation

imparts a larger impact on $R_{rs}(\lambda)$ variation than does cell size, but we do not have a clear understanding of how much larger the impact is or how variable it can be. By holding chlorophyll at the annual mean, we were able to isolate and understand the impact of size variation in the absence of chlorophyll variation, which could have otherwise confused our interpretation.

The second case study was performed to understand seasonal and spatial variability where $R_{rs}(\lambda)$ was being significantly impacted by phytoplankton size composition. This case study was performed using 2004 monthly CCSM-3 BEC output. Two scenarios were performed in this case study, 1) full cell size and chlorophyll concentration variability, where phytoplankton absorption varies due to phytoplankton cell size (size-dependent) and, 2) chlorophyll concentration variability only; phytoplankton chlorophyll-specific absorption was held constant, thus absorption did not change with variation in cell size (size-independent absorption). The constant chlorophyll-specific absorption was considered in two ways. First, the constant chlorophyll-specific absorption spectra utilized in the size-independent absorption scenario was calculated as the mean of the micro-, ultra-, nano- (Ciotti et al., 2002), and picoplankton (Ciotti and Bricaud, 2006) chlorophyll-specific absorption spectrum (herein referred to as Ciotti average) (Fig. 3). Second, the constant chlorophyll-specific absorption was determined from equation 5 when using the model mean S_{fm} (35%). As prescribed by the above optical model, the distribution of chlorophyll between the phytoplankton size classes (i.e. S_f and S_{fm}, equation 4) determines the chlorophyll-specific absorption spectra (equation 5) in the full variability scenario. Satellite algorithms and optical models often assume constant average chlorophyll-specific phytoplankton absorption spectra. This case study aims to demonstrate when and where

this assumption does not hold true. In each of the scenarios only the parameters of interest were changed; all other optical parameters were treated identically.

2.5 Analysis methods

The analysis focused on the overall $R_{rs}(\lambda)$ resulting from each optical scenario. All of the resulting R_{rs} spectra were normalized to 555 nm (referred to as $\hat{R}_{rs}(\lambda)$ from this point forward, units are dimensionless) to focus on the shape of the spectra and emphasize the magnitude shift between pico- and microplankton at the 443 nm band (Mouw and Yoder, 2010). The band 555 nm was chosen to normalize the spectra because phytoplankton absorption was the lowest at this band. The greatest difference in absorption related to phytoplankton cell size was observed at 443 nm, thus our analysis is focused on this band (Fig. 5). To compare scenarios with constant chlorophyll ($\hat{R}_{rs}(\lambda)_{chl}$), constant phytoplankton size ($\hat{R}_{rs}(\lambda)_{S_{fm}}$), or constant chlorophyll-specific absorption ($\hat{R}_{rs}(\lambda)_{Ciotti-avg}$ or $\hat{R}_{rs}(\lambda)_{indep-mean}$) to those with full model variability ($\hat{R}_{rs}(\lambda)_{dep-a}$ or $\hat{R}_{rs}(\lambda)_{dep-m}$), we calculated for each scenario percent fractional error ($[(\hat{R}_{rs}(443)_{chl}$ (or $\hat{R}_{rs}(443)_{S_{fm}}) - \hat{R}_{rs}(443)_{dep-a})/\hat{R}_{rs}(443)_{dep-a}] \times 100$) or percent difference ($\{(\hat{R}_{rs}(443)_{Ciotti-avg} - \hat{R}_{rs}(443)_{dep-m}) / [(\hat{R}_{rs}(443)_{Ciotti-avg} + \hat{R}_{rs}(443)_{dep-m})/2]\} \times 100$). The use of percent fractional error or percent difference allows the analysis to only focus on the portion of the $\hat{R}_{rs}(\lambda)$ that changed due to $[Chl_{size}]$, S_{fm} or absorption effects.

3. Results

3.1 First case study: annual constant chlorophyll and constant phytoplankton size scenarios

The variation in the spectral shape of the global annual mean normalized reflectance spectra was compared in Figure 6 for three scenarios: the cell size dependent, full variability case ($\hat{R}_{rs}(\lambda)_{dep-a}$), the global mean constant [Chl_{size}] (0.17 mg m^{-3}) case ($\hat{R}_{rs}(\lambda)_{chl}$), and the global mean constant S_{fm} (35%) case ($\hat{R}_{rs}(\lambda)_{S_{fm}}$). Figure 6 also displays for each case the envelope encompassing one standard deviation about each spectral curve. One standard deviation of the spectral variability of $\hat{R}_{rs}(\lambda)_{chl}$ fell completely within one standard deviation of $\hat{R}_{rs}(\lambda)_{S_{fm}}$. This indicates that $\hat{R}_{rs}(\lambda)$ variability due to chlorophyll is greater than that due to cell size alone; however, $\hat{R}_{rs}(\lambda)$ variability due to S_{fm} is important as a secondary effect. As chlorophyll concentration increases, the peak of the maximum $\hat{R}_{rs}(\lambda)$ shifts to longer wavelengths (O'Reilly et al., 1998). Changes in $\hat{R}_{rs}(\lambda)$ due to cell size variations primarily alter the magnitude of the curve rather than shifting of the peak wavelength. The greatest $\hat{R}_{rs}(\lambda)$ difference in magnitude was found at 443 nm (Mouw and Yoder, 2010); thus we focused our quantification efforts primarily at 443 nm. At 443 nm, the mean (standard deviation) for $\hat{R}_{rs}(443)_{dep-a}$, $\hat{R}_{rs}(443)_{chl}$, and $\hat{R}_{rs}(\lambda)_{S_{fm}}$ was 3.31 (0.36), 3.15 (0.14), and 3.19 (0.46), respectively.

To further explore the difference between $\hat{R}_{rs}(443)_{dep-a}$, $\hat{R}_{rs}(443)_{chl}$, and $\hat{R}_{rs}(\lambda)_{S_{fm}}$, scatter plots for each of these scenarios were compared (Fig. 7). To help visualize the general trend of each scenario, a linear regression was fit. The regressions for $\hat{R}_{rs}(443)_{dep-a}$ versus $\hat{R}_{rs}(\lambda)_{S_{fm}}$ and $\hat{R}_{rs}(443)_{dep-a}$ versus $\hat{R}_{rs}(443)_{chl}$ resulted in correlation coefficients (r^2) of 0.74 and 0.29, root mean square error (RMSE) of 0.529 and 0.587, slopes of 0.887 and 0.374, and intercepts of 0.278 and 1.888, respectively (Fig. 7). The divergence of points from the 1:1 line,

and the divergence of the statistically fitted regression line from the 1:1 line, indicates the extent to which grid-point $\hat{R}_{rs}(443)$ values differed when a single parameter was held constant relative to the full variability $\hat{R}_{rs}(443)$ simulation. While there was significant variability about the regression fits, the linear regressions and scatter plots indicated that the deviations from $\hat{R}_{rs}(443)_{dep-a}$ were larger for the $\hat{R}_{rs}(443)_{chl}$ scenario than for the $\hat{R}_{rs}(\lambda)_{S_{fm}}$ scenario; there is also considerably more structure in fit residuals in the $\hat{R}_{rs}(443)_{chl}$ scenario, with positive biases at low $\hat{R}_{rs}(443)$ and negative biases at high $\hat{R}_{rs}(443)$. This indicated that geographic variations in chlorophyll concentration impact $\hat{R}_{rs}(443)$ more significantly than geographic variations in cell size or S_{fm}.

To quantify the relative impact of S_{fm} and [Chl_{size}] on $\hat{R}_{rs}(443)$ we calculated their respective percent fractional error. Percent fractional error was determined at each model grid cell from $\hat{R}_{rs}(443)_{dep-a}$, $\hat{R}_{rs}(443)_{chl}$, and $\hat{R}_{rs}(443)_{S_{fm}}$ (for example, S_{fm} percent fractional error was calculated as: $[(\hat{R}_{rs}(443)_{S_{fm}} - \hat{R}_{rs}(443)_{dep-a})/\hat{R}_{rs}(443)_{dep-a}] \times 100$) (Fig 8). The magnitude of the contribution of [Chl_{size}] on $\hat{R}_{rs}(443)_{dep-a}$ was much greater than that due to S_{fm}. The sign of the percent fractional error between [Chl_{size}] and S_{fm} was generally opposite for a given region of the ocean. Assuming a fixed chlorophyll concentration, the optical model resulted in a large positive error or bias in $\hat{R}_{rs}(443)_{dep-a}$ at mid- to high-latitudes and a negative bias in the subtropics. The percent fractional errors in assuming a constant phytoplankton size tended to be smaller in magnitude and generally opposite in sign, with positive biases in the tropics and subtropics (+10 to +20%) and negative biases in temperate to polar environments (-10 to -40%).

3.2 Second case study: monthly size-dependent and size-independent absorption scenarios

We were primarily interested in the difference between the size-independent (using the Ciotti average chlorophyll-specific absorption spectra) ($\hat{R}_{rs}(443)_{Ciotti-avg}$) and size-dependent (full variability) ($\hat{R}_{rs}(443)_{dep-m}$) scenarios, we first calculated the percent difference between these scenarios for each pixel of the monthly model output:

$$\{(\hat{R}_{rs}(443)_{Ciotti-avg} - \hat{R}_{rs}(443)_{dep-m}) / [(\hat{R}_{rs}(443)_{Ciotti-avg} + \hat{R}_{rs}(443)_{dep-m})/2]\} \times 100 \qquad (17)$$

The annual mean percent difference global field (Fig. 9) was then subtracted from each of the monthly fields, and the monthly deviation maps were compared (Fig. 10).

Considering first the mean field, the highest values for the positive mean percent difference between $\hat{R}_{rs}(443)_{Ciotti-avg}$ and $\hat{R}_{rs}(443)_{dep-m}$ were found in the tropical and subtropical Atlantic and Indian Oceans, the central gyres and equatorial region of the Pacific Ocean (Fig. 9). A positive percent difference was found across much of the global ocean, with the exception of portions of the Southern Ocean, the Arctic Ocean and southeast of Greenland in the North Atlantic. Global fields of $\hat{R}_{rs}(443)_{Ciotti-avg}$ were on average 14% higher than $\hat{R}_{rs}(443)_{dep-m}$ (Fig. 9, Table 2). This indicated that on average, the Ciotti-average chlorophyll-specific absorption was lower (higher S_{fm}) than the size-dependent scenario. In other words, a positive percent difference resulted when the chlorophyll-specific absorption for the size-dependent scenario was higher (lower S_{fm}) than the chlorophyll-specific absorption for the size-independent Ciotti-average scenario. This suggests that over the majority of the ocean, the model phytoplankton assemblage contains a greater percentage of picoplankton than that associated with the Ciotti-average chlorophyll-specific absorption. In the high latitudes of the Southern and Arctic Oceans and also southeast of Greenland, the negative percent difference between Ciotti-average and

size-dependent scenarios indicated that the size-dependent scenario had a greater percentage of large cells (higher S_{fm}), lower chlorophyll-specific absorption, and thus higher $\hat{R}_{rs}(443)$ than the Ciotti-average scenario.

Two main patterns emerge from the monthly percent difference deviation maps. First, there are seasonal changes to the size-independent (using the Ciotti-average chlorophyll-specific absorption spectra) ($\hat{R}_{rs}(443)_{Ciotti-avg}$) and size-dependent (full variability) ($\hat{R}_{rs}(443)_{dep-m}$) scenarios throughout the global ocean. Second, seasonal deviations are generally much larger in higher latitudes than elsewhere, particularly in the Southern Ocean.

Briefly, April and November were transitional months in the subtropical ocean, with generally negative deviations in the local spring through early fall months in both hemispheres. The sub-polar deviations were opposite in sign compared to the subtropical ocean with positive deviations in the local summer to fall months between hemispheres. The Arctic Ocean displayed positive deviations only in the brief summer months. The Southern Ocean consistently had strong anomalous patches persistent throughout the year, with the patches displaying opposing signs in November through March compared to April through October. In other words, phytoplankton size effects act to increase $\hat{R}_{rs}(443)$ over the subtropical oceans in both hemispheres during the local spring through early fall months, decrease $\hat{R}_{rs}(443)$ during local winter months. At high latitudes in the NH, size effects increase $\hat{R}_{rs}(443)$ for December through April and decrease $\hat{R}_{rs}(443)$ for May through November. The very patchy Southern Ocean made generalizations about this region difficult.

3.2.1 Correlation Analysis

Correlation analysis was performed and the r^2 was mapped between monthly

$\hat{R}_{rs}(443)_{dep-m}$ and [Chl_{size}] (Fig. 11a), [Chl_{size}] and S_{fm} (Fig. 11b), and $\hat{R}_{rs}(443)_{dep-m}$ and S_{fm} (Fig. 11c). As expected, the seasonal correlation between $\hat{R}_{rs}(443)_{dep-m}$ and [Chl_{size}] was strongly negative across the majority of the global ocean (-0.87) (Fig. 11a, Table 3). The reason for the negative relationship is that chlorophyll concentration increases phytoplankton absorption, thus decreasing $\hat{R}_{rs}(443)_{dep-m}$. Over most of the ocean, [Chl_{size}] and S_{fm} are in phase seasonally; meaning seasonal blooms were associated with an increase in microplankton. The exception to this was found in the subpolar North Pacific and subpolar and polar Southern Ocean (Fig. 11b). An increase in [Chl_{size}] or S_{fm} independent of any other change would have opposite effects on $\hat{R}_{rs}(443)_{dep-m}$. In the large part of the global domain, where [Chl_{size}] and S_{fm} are positively correlated, the net effect on the seasonal variation in $\hat{R}_{rs}(443)_{dep-m}$ depends on the strength of the seasonal variation of [Chl_{size}] to S_{fm}. The seasonal correlation between $\hat{R}_{rs}(443)_{dep-m}$ and S_{fm} was generally both highly negative in the tropics and subtropics and highly positive at high latitudes (Fig. 11c). Low seasonal correlation was found in the transitional zones between the subtropical and polar regions and in much of the western Pacific. Examining all three panels of Fig. 11 suggested that S_{fm} was largely secondary to [Chl_{size}] in forcing seasonal variations of $\hat{R}_{rs}(443)_{dep-m}$ and that the sign of the correlation of S_{fm} and $\hat{R}_{rs}(443)_{dep-m}$ (Fig. 11c) reflects primarily the underlying regional relationships between S_{fm} and [Chl_{size}] (Fig. 11b) and the strong global anti-correlation of $\hat{R}_{rs}(443)_{dep-m}$ and [Chl_{size}].

3.2.2 Chlorophyll Concentration Analysis

To portray the size-dependent and size-independent scenarios in a more familiar way, the ocean color 4-band ratio (OC4) algorithm for chlorophyll concentration was calculated from the

monthly remote sensing reflectance for Ciotti-average size-independent ($R_{rs}(\lambda)_{Ciotti-avg}$), model mean size-independent ($R_{rs}(\lambda)_{indep-mean}$) and size-dependent ($R_{rs}(\lambda)_{dep-m}$) optical output. OC4 is the standard chlorophyll algorithm used when processing SeaWiFS imagery and is an empirically fit polynomial that utilizes band shifting to longer wavelengths with increasing chlorophyll concentration (O'Reilly et al., 1998). The global 2004 annual mean OC4 [Chl] for the Ciotti-average size-independent, model mean size-independent (i.e. equation 5 when S_{fm} is set constant at 35%) and size-dependent absorption simulations were 0.174, 0.219 and 0.216 mg m^{-3}, respectively (Table 2). This resulted in an annual average -21.5% and 1.4% difference in OC4 [Chl] estimates from the size-dependent scenario for the Ciotti-average size-independent and model mean size-independent scenarios, respectively (Fig. 12; Table 2). The difference between the size-dependent and Ciotti-average size-independent estimates is not just an overall mean bias; the Ciotti-average size-independent OC4 [Chl] estimates displayed a greater magnitude change in the subtropical to temperate gradient compared to the size-dependent OC4 [Chl] estimates. Over most of the global ocean the annual size-dependent OC4 [Chl] estimates were on average 15% to 30 % higher than the annual Ciotti-average size-independent OC4 [Chl] estimates. However, in the central gyre of the North Atlantic, the annual size-dependent OC4 [Chl] estimates are approximately 50% higher than the annual size-independent OC4 [Chl] estimates. Conversely, in the Southern Ocean and high latitudes of the North Atlantic, the size-dependent OC4 [Chl] estimates are equal to or up to 20% lower than the annual size-independent OC4 [Chl] estimates (Fig. 12d). The low percent difference between the size-dependent and model mean size-independent scenarios is related to the positive difference in the high latitudes, but negative difference in the low latitudes (Fig. 12e). The distinct zonal regions occur because the model mean size-independent scenario represents a picoplankton-dominated case, which is closer to

CCSM-3 BEC model's size distribution in low latitudes. The model mean size-independent scenario was considered to understand the bias present when choosing a chlorophyll-specific absorption spectra not associated with the model mean conditions. The bias was examined by differencing the Ciotti-average size-independent percent difference with the model mean size-independent percent difference. The mean annual bias is -22%. The lowest bias is found in the Southern Ocean, the high latitudes of the North Atlantic and across much of the low latitudes with the exception of the equatorial upwelling region and the southern portion of the North Atlantic gyre. The greatest bias is observed in the mid-latitudes particularly west of Argentina, south of Australia and in the northern portion of the North Pacific gyre (Fig. 12f).

The monthly temporal changes in OC4 [Chl] percent difference between the size-dependent and Ciotti-average size-independent scenarios were considered. Keeping in mind the negative percent difference bias between the Ciotti-average and model mean size-independent scenarios, [Chl] is underestimated when S_{fm} is elevated, which generally occurs at high latitudes in the local spring and summer. Specifically, in the low to mid latitude regions, size-dependent OC4 [Chl] estimates were generally 30-60% higher than the Ciotti-average size-independent OC4 [Chl] estimates across all months. In the high latitude regions, size-dependent OC4 [Chl] estimates were 50-150% lower than the Ciotti-average size-independent OC4 [Chl] estimates during local spring to summer months. During local winter months at high latitudes, the size-dependent and size-independent OC4 [Chl] estimates at high latitudes were nearly equal (Fig. 13). There are known spatial biases in the CCSM-3 BEC model that will be reflected here (Doney et al., 2009), thus the spatial distribution is not expected to look identical to satellite retrievals of OC4 [Chl]. For band-ratio algorithms, such as OC4, an increase in S_{fm} effectively looks like a decrease in chlorophyll concentration. If as in the CCSM-3 BEC, chlorophyll

concentration and phytoplankton size are positively correlated over most of the global domain, the impact by cell size has the effect of dampening large-scale spatial gradients.

4. Discussion and Conclusions

The focus of this study was to understand the impact of phytoplankton cell size and chlorophyll concentration on $R_{rs}(\lambda)$ using models to approximate the global variation and co-variation in phytoplankton cell size (two size classes only) and chlorophyll concentration that occurs in nature. We were not overly concerned with the model's agreement with *in situ* or satellite data; these issues are treated elsewhere (Doney et al., 2009). The CCSM-3 BEC model represents a global coincident estimate in space and time of phytoplankton cell size, chlorophyll concentration, and other pertinent ecosystem state variables that are dynamically consistent and unattainable by any other approach owing to a paucity of global *in situ* observations. These estimated parameters were exploited as a means to isolate variation in $R_{rs}(\lambda)$ due to changes in phytoplankton size and chlorophyll concentration over a reasonable range of global variability. It is important to point out that assumptions in the optical model were used to obtain a best guess, such as some of the spectral shape coefficients, backscattering efficiency, and the conversion from DOC to $a_{CDM}(\lambda_o)$. Comparisons were made directly between full variability output and sensitivity experiments with a single parameter altered (with all other optical parameters treated identically between scenarios) isolating only the effect on remotely sensed reflectance resulting from the altered parameter.

Compared to chlorophyll concentration, phytoplankton size imparts a secondary impact on remotely sensed reflectance in the model and by implication, in nature. Globally, the magnitude of the percent fractional error of S_{fm} on $\hat{R}_{rs}(443)_{dep-a}$ was lower than the percent

fractional error of [Chl_{size}], and generally opposite in sign. High latitude regions expressed the greatest impact on $\hat{R}_{rs}(443)$ due to phytoplankton size. $\hat{R}_{rs}(443)$ was impacted by both [Chl_{size}] and S_{fm} (although in opposite sign) in regions influenced by large scale upwelling and monsoon dynamics, however impact due to S_{fm} was smaller in magnitude. The correlation between [Chl_{size}] and S_{fm} indicate that these two parameters were generally positively coupled over the seasonal cycle in low latitude regions. This indicates that seasonal increases in chlorophyll in low latitude regions were generally accompanied by increases in larger phytoplankton cells within the phytoplankton assemblage. At very high latitudes, there are regions in the CCSM-3 BEC simulation where S_{fm} and [Chl_{size}] are strongly anti-correlated and other regions where correlation is poor. These results suggest that at high latitudes, the idea that increases in chlorophyll concentration is largely related to an increase in the percentage of large cells, does not hold true, at least in this particular ecosystem model.

A comparison of $\hat{R}_{rs}(443)$ in simulations with constant chlorophyll-specific absorption spectra (and thus constant size structure) ($\hat{R}_{rs}(443)_{Ciotti-avg}$) against full time and space varying phytoplankton size structure ($\hat{R}_{rs}(443)_{dep-m}$) indicated positive percent differences across the tropical and subtropical global ocean. These differences result from the community structure in the CCSM-3 BEC model consisting of a greater percentage of pico- and nanoplankton, thus resulting in a higher chlorophyll-specific absorption (and lower $\hat{R}_{rs}(443)$) than the Ciotti average absorption. In a converse example, the only negative percent difference between $\hat{R}_{rs}(443)_{Ciotti-avg}$ and $\hat{R}_{rs}(443)_{dep-m}$ was found in the Southern and Arctic Oceans and southeast of Greenland in the North Atlantic. In these cases, the phytoplankton community in the CCSM-3 BEC model was comprised of cells larger than those associated with the Ciotti-average chlorophyll-specific

absorption, resulting in lower size-dependent chlorophyll-specific absorption and higher $\hat{R}_{rs}(443)_{dep-m}$.

As explained previously, loosely packaged microphytoplankton (i.e. high S_{fm}), absorb comparatively less light per unit chlorophyll. Conversely, tightly packaged picoplankton (i.e. low S_{fm}), absorb comparatively more light per unit chlorophyll and tend to be associated with low [Chl_{size}]. Thus, the same high $\hat{R}_{rs}(443)$ can result from two different conditions: (1) low S_{fm} in low [Chl_{size}] regions of the ocean such as the Sargasso Sea, or high S_{fm} and moderate [Chl_{size}] such as in the Southern Ocean.

Most biogeochemistry/ecosystem/circulation models predict [Chl] not $R_{rs}(\lambda)$. This can lead to complications in the comparison of model output with observations of remotely sensed properties because the uncertainty of satellite derived [Chl] is much higher than the uncertainty associated with $R_{rs}(\lambda)$. However, a straight comparison of model and satellite observed chlorophyll concentration is appropriate as long as the observational approach takes phytoplankton size into account either empirically or semi-empirically. The spatial changes in percent fractional error and the spatial and temporal changes in percent difference indicate variations in phytoplankton size can substantially impact $\hat{R}_{rs}(443)$. High latitudes are particularly susceptible to under and overestimation of remote sensing reflectance. When not considering phytoplankton size effects, $\hat{R}_{rs}(443)$ will be underestimated in the subtropical oceans in both hemispheres during local spring through early fall months and overestimated during local winter months. The high latitudes are generally out of phase with each other; underestimation occurred during the local winter months and overestimation during the local summer months, with the deviations being stronger and patchier in the Southern Ocean. When applying band-ratio algorithms, remote sensing reflectance and chlorophyll concentration are empirically

related; thus an impact on $R_{rs}(\lambda)$ by phytoplankton size will also impact [Chl] estimates. In general, our calculations from model output indicate that when phytoplankton size effects are not considered, [Chl] will be on average underestimated by standard satellite algorithms (e.g. OC4). These results have important implications as to when and where the satellite standard algorithms will either overestimate or underestimate [Chl] due to $R_{rs}(443)$ being significantly affected by phytoplankton size. As [Chl] increases, phytoplankton absorb more light, resulting in decreased $R_{rs}(443)$. Thus in tune with the $R_{rs}(443)$ seasonal changes, we expect the OC4 algorithm will overestimate [Chl] during in the tropical and subtropical oceans in both hemispheres during local spring through early fall months and underestimate during local winter months. At high latitudes, we expect [Chl] will be overestimated during the local winter and underestimated during the local summer. The impact of cell size variability on $R_{rs}(\lambda)$ was not a factor in the development of the OC4 relationship between $R_{rs}(\lambda)$ and [Chl] but it is indirectly encapsulated due to the inclusion [Chl] associated with various phytoplankton assemblages across the global ocean. However, the OC4 empirical relationship is a regression fit that cannot capture the full variability between chlorophyll concentration and $R_{rs}(\lambda)$. This study attempts to tease apart where and when the variability about the OC4 relationship may be associated with cell size variability rather than chlorophyll variability alone. The monthly OC4 [Chl] calculations from the model simulated output generally indicated that when not considering cell size, [Chl] in low to mid latitudes regions was overestimated throughout the year and at high latitudes, [Chl] was underestimated during the local spring to summer months.

We found that considering size-varying phytoplankton absorption in an optical model resulted in the global average $\hat{R}_{rs}(443)$ and OC4 [Chl] calculations with 14% lower and 22% higher than when holding phytoplankton absorption constant. The difference between scenarios

reflects the impact phytoplankton size has on remote sensing reflectance and chlorophyll estimates, in addition to the difference between the CCSM-3 BEC model's output phytoplankton size structure compared to the Ciotti-average estimate. More work is needed to quantify the size-structure from observations and to evaluate and improve model predictions of size structure. The negative seasonal correlation between [Chl] and $R_{rs}(443)$ is indisputable and has been utilized in standard satellite algorithms (O'Reilly et al., 1998). However, the relationship of S_{fm} to $R_{rs}(\lambda)$ has not been extensively explored. In the model results, we found that S_{fm} also was generally strongly correlated with $\hat{R}_{rs}(443)_{dep-m}$, but the sign of the relationship varied with location. $[Chl_{size}]$ and S_{fm} were positively seasonally correlated at low to mid-latitudes, while the relationship was either anti- or poorly seasonally correlated in high latitudes. This implies the equatorial and subtropical regions of the ocean have an in-phase (positive) relationship between [Chl] and S_{fm} in that [Chl] and S_{fm} tend to increase together. The correlation sign reversal (negative) at high latitudes implied that decreases in $\hat{R}_{rs}(443)_{dep-m}$ may be caused by a shift to larger phytoplankton cells as well as an increase in [Chl].

There are many implications of adding optics to biogeochemistry / ecosystem / circulation models. Previous physical-ecosystem modeling studies that have implemented an optical model found better agreement with in situ observations than models that did not consider optics (Bissett et al., 1999a; Bissett et al., 1999b; Fuji et al. 2007). In the present study, the implementation was in an off-line diagnostic manner. In this way, we were able to isolate potential knowledge gained from specific manipulation of the optical model. We have learned that explicitly considering phytoplankton cell size can significantly alter the outcome of modeling efforts. There is potential to gain considerable knowledge about other optically active constituents through additional linear coupling of ecosystem numerical output with optical

models. This effort constitutes a step toward understanding the implications of linking two traditionally independent fields of study.

One of the challenges in developing marine biogeochemical/ecosystem models is the lack of data with adequate spatial and temporal resolution for calibration and validation. Satellite chlorophyll data has helped tremendously to address this issue (Bennington et al., 2009; Lima and Doney, 2004; Moore et al., 2002a; Tjiputra et al., 2007). However, beyond chlorophyll concentration, an advantage gained in the use of an optical model is a greater suite of parameters to validate and constrain the biogeochemistry/ecosystem model. The greatest utility in a combined ecosystem-optical model comes at a fundamental level of comparison between satellite observations and model output. As much as possible, we want to compare model results to actual observations rather than derived products. Satellite derived products, such as chlorophyll concentration, have inherent error greater than the error associated with the observed parameter, in this case, remote sensing reflectance. If we understand the optical coefficients such as total scattering and absorption resulting from the CCSM-3 BEC model, we have greater power over the interpretation and are left with fewer uncertainties related to empirical fits. We could compare the resultant $R_{rs}(\lambda)$ from the combined ecosystem-optical model to satellite radiometry measurements and move beyond satellite derived chlorophyll for model validation. The uncertainty of the satellite measured $R_{rs}(\lambda)$ is significantly lower than that of the standard OC4 chlorophyll concentration product (Bailey and Werdell, 2006).

Looking ahead to the intersection of optics and ecosystem modeling, the ideal junction of these two traditionally independent fields lies in a feedback of the optics into the ecosystem model to improve the accuracy of modeling of the underwater light field, which will ultimately produce more accurate optical, biogeochemical and ecosystem parameter output.

Biogeochemical / ecosystem / circulation models of the ocean are essential tools for understanding the global carbon cycle, while remotely sensed optical properties offer the most comprehensive spatial and temporal view of the ocean surface. The data-poor constraint and tuning of many numerical models can only benefit from exploiting one of our most data-rich sources of ocean observation, remote sensing. The combination of these two fields of research represent, on the long term, a key opportunity to improve our understanding of links between variability and change in climate, ecosystems and biogeochemistry.

In conclusion, we found that while phytoplankton cell size effects on $R_{rs}(\lambda)$ were secondary to chlorophyll concentration, the impact can be substantial in upwelling and deep mixing regions of the ocean. Differences between the various scenarios have lent insight into the importance of considering phytoplankton size when interpreting remote measurements of $R_{rs}(\lambda)$. By implication, the results also give insight into the possible errors in estimating chlorophyll concentration from R_{rs} when considering a global phytoplankton population having size-independent mean absorption properties. The latter is the common assumption when interpreting R_{rs} from satellite measurements. This study points to the importance of understanding the ecological structure of phytoplankton communities, beyond just biomass, and lends credence to the accomplishments and on-going developments of phytoplankton size retrieval from satellite observations.

Acknowledgments

We would like to thank I. Lima for assistance in generating the CCSM-3 BEC model output and for helpful discussions. We would like to thank the SeaWiFS Project at NASA GSFC for the processing and distribution of the SeaWiFS monthly mapped $nL_w(\lambda)$ imagery. This manuscript benefited from discussions with G. McKinley, T. Rynearson, Y. Wang, and J. O'Reilly. Funding for this study came from a NASA Earth and Space Science Fellowship and University of Rhode Island Graduate School Oceanography Alumni Fellowship, both awarded to C. Mouw. The CCSM-3 BEC simulations were generated with support from NASA Ocean Biology and Biogeochemistry Program (NNX07AL80G) and the NSF Center for Microbial Oceanography Research and Education (C-MORE, EF-0424599).

References

Antoine, D., Morel, A., Gordon, H. R., Banzon, V.F., Evans, R. H., 2005. Bridging ocean color observations of the 1980s and 2000s in search of long-term trends. J. Geophys. Res. 110, C06009, doi: 1029/2004JC002620.

Bailey, S. W., Werdell, P. J., 2006. A multi-sensor approach for the on-orbit validation of ocean color satellite data products. Remote Sens. Environ. 102, 12-23.

Barnard, A. H., Pegau, W. S., Zaneveld, J. R. V., 1998. Global relationships of the inherent optical properties of the oceans. J. Geophys. Res. 103, 24955-24968.

Behrenfeld, M. J., Boss,E., Siegel, D.A., Shae, D.A., 2005. Carbon-based ocean productivity and phytoplankton physiology from space. Global Biogeochem. Cycles. 19, GB1006, doi: 1010.1029/2004GB002299.

Bennington, V., McKinley, G.A., Dutkiewicz, S., Ullman, D., 2009. What does chlorophyll variability tell us about export and CO2 flux variability? Global Biogeochem. Cycles. 23, GB3002, doi:10.1029/2008GB003241.

Bissett, W. P., Carder, K. L., Walsh, J. J., Dieterle, D.A., 1999a. Carbon Cycling in the upper waters of the Sargasso Sea: II. Numerical simulation of apparent and inherent optical properties. Deep Sea Res. Part I Oceanogr. Res. Pap. 46, 271-317.

Bissett, W. P., DeBra, S., Dye, D., 2004. Ecological simulation (EcoSim) 2.0 technical description, Florida Environmental Research Institute.

Bissett, W. P., Schofield, O., Glenn, S., Cullen, J.J., Miller, W.L., Plueddemann, A.J., Mobley, C.D., 2001. Resolving the Impacts and Feedback of ocean optics on upper ocean ecology. Oceanography. 14, 30-49.

Bissett, W. P., Walsh, J. J., Dieterle, D.A., Carder, K.L., 1999b. Carbon cycling in the upper waters of the Sargasso Sea: I. Numerical simulation of differential carbon and nitrogen fluxes. Deep Sea Res. Part I Oceanogr. Res. Pap. 46, 205-269.

Bopp, L., Monfray, P. Aumont, O., Dufresne, J.-L., Le Treut, H., Madec, G., Terray, L., Orr, J.C., 2001. Potential impact of climate change on marine export production. Global Biogeochem. Cycles. 15, 81-99.

Bracher, A., Vountas, M., Dinter, T., Burrows, J.P., Röttgers, R., Peeken, I., 2009. Quantitative observation of cyanobacteria and diatoms from space using PhytoDOAS on SCIAMACHY data. Biogeosciences, 6, 751-764.

Bricaud, A., Morel, A., Prieur, L., 1983. Optical efficiency factors of some phytoplankters. Limnol. Oceanogr. 28(5), 816-832.

Carder, K.L., Chen, F.R., Lee, Z.P. and Hawes, S.K., 1999. Semianalytic Moderate-Resolution Imaging Spectrometer algorithms for chlorophyll a and absorption with bio-optical domains based on nitrate-depletion temperatures. J. Geophys. Res. 104 (C3), 5403-5421.

Ciotti, A., Lewis, M., Cullen, J., 2002. Assessment of the relationship between dominant cell size in natural phytoplankton communities and the spectral shape of the absorption coefficient. Limnol. Oceanogr. 47(2), 404-417.

Ciotti, A. M., Bricaud, A., 2006. Retrievals of a size parameter for phytoplankton and spectral light absorption by colored detrital matter from water-leaving radiances at SeaWiFS channels in a continental shelf region off Brazil. Limnol. Oceangr. Methods. 4, 237-253.

Collins, W. D. Blackmon, M., Bitz, C.M., Bosnan, G.B., Bretherton, G.B., Carton, C.S., Chang, P. Doney, S.C., Hack, J.J., Kiehl, J.T., Henderson, T., Large, W.G., McKenna, D., Santer, B.D., 2006. The Community Climate System Model: CCSM3. J. Climate. 19, 2122-2143.

Dickey, T., Lewis, M. R., Chang, G.C., 2006. Optical oceanography: recent advances and future directions using global remote sensing and in situ observations. Rev. Geophys. 44, RG1001, doi: 10.1029/2003RG000148.

Doerffer, R., Schiller, H., 2007. The MERIS Case 2 water algorithm. Internat. J. Remote Sens. 28(3), 517-535.

Doney, S. C., Lima, I., Moore, J.K., Lindsay, K., Behrenfeld, M.J., Westberry, T.K., Mahowald, N., Glover, D.M., Takahaski, T., 2009. Skill metrics for confronting global upper ocean ecosystem-biogeochemistry models against field and remote sensing data. J. Mar. Syst. 76, 95-112.

Doney, S. C.,Lindsay, K., Fung, I., John, J., 2006. Natural variability in a stable 1000 year coupled climate-carbon cycle simulation. J. Climate. 19, 3033-3054.

Doney, S. C., Yeager, S., Danabasoglu, G., Large, W.G., McWilliams, J.C., 2007. Mechanisms governing interannual variability of upper ocean temperature in a global hindcast simulation. J. Phys. Oceanogr. 37, 1918-1938.

Duysens, L. N. M. 1956. The flattening of the absorption spectrum of suspensions, as compared to that of solutions. Biochim. Biophys. Acta. 19, 1-12.

Fujii, M., Boss, E., Chai, F., 2007. The value of adding optics to ecosystem models: a case study. Biogeosciences. 4, 817-835.

Geider, R., MacIntyre, H., Kana, T., 1998. A dynamic regulatory model of phytoplanktonic acclimation to light, nutrients, and temperature. Limnol. Oceangr. 43(4), 679-694.

Gregg, W. W., Casey, N. W., McClain, C.R., 2005. Recent trends in global ocean chlorophyll. Geophys. Res. Let. 32, L03606, doi: 10.1029/2004GL021808.

Gregg, W. W., Casey, N.W., 2009. Skill assessment of a spectral ocean-atmosphere radiative model. J. Mar. Syst. 76, 49-63.

Henson, S.A., Sarmiento, J.L., Dunne, J.P., Bopp, Lima, I. L., Doney, S.C., John, J., Beaulieu, C., 2010. Detection of anthropogenic climate change in satellite records of ocean chlorophyll and productivity. Biogeosciences, 7(2), 621-640.

Hirata, T., Aiken, J., Hardman-Mountford, N., Smyth, T.J., Barlow, R.G., 2008. An absorption model to determine phytoplankton size classes from satellite ocean color, Remote Sens. Environ., 112, 3153-3159.

Kostadinov, T.S., Siegel, D.A., Maritorena, S., 2009. Retreival of the particle size distribution from satellite ocean color observations, J. Geophys. Res. 114, C09015, doi:10.1029/2009JC005303.

Kostadinov, T.S., Siegel, D.A., Maritorena, S., 2010. Global variability of phytoplankton functional types from space: assessment via the particle size distribution. Biogeosci. 7, 3239-3257.

Lima, I. D., Doney, S.C., 2004. A three-dimensional, multinutrient, and size-structured ecosystem model for the North Atlantic. Global Biogeochem. Cycles. 18, GB3019, doi: 10.1029/2003GB002146.

Liu, C.-C., Woods, J.D., Mobley, C.D., 1999. Optical model for use in oceanic ecosystem models. Appl. Opt. 38, 4475-4485.

Mahowald, N., Luo, C., Corral, J. D., Zender, C., 2003. Interannual varaibility in atmospheric mineral aerosols from a 22-year model simulation and obsservational data. J. Geophys. Res. 108, 4352.

Maritorena, S., Siegel, D. A., Peterson, A.R., 2002. Optimization of a semianalytical ocean color model for global-scale applications. Appl. Opt. 41, 2705-2714.

Mobley, C. D., 1989. A numerical model for the computation of radiance distributions in natural waters with wind-roughened surfaces. Limnol. Oceangr. 34, 1473-1483.

Mobley, C. D., 1994. Light and Water. Academic, San Diego.

Mobley, C. D., Sundman, L. K., 2008a. Hydrolight 5 Technical Documentation, Sequoia Scientific.

Mobley, C. D., Sundman, L. K., 2008b. Hydrolight 5 Users' Guide, Sequoia Scientific.

Moore, J.K., Doney, S.C., Glover, D.M., Fung, I.Y., 2002a. Iron cycling and nutrient-limitation patterns in surface waters of the World Ocean. Deep Sea Res. Part II Top. Stud. Oceanogr. 49, 463-507.

Moore, J.K., Doney, S.C., Kleypas, J.A., Glover, D.M., Fung, I.Y., 2002b. An intermediate complexity marine ecosystem model for the global domain. Deep Sea Res. Part II Top. Stud. Oceanogr. 49, 403-462.

Moore, K. J., Doney, S.C., Lindsay, K., 2004. Upper ocean ecosystem dynamics and iron cycling in a global three-dimensional model. Global Biogeochem. Cycles. 18, GB4028.

Morel, A., 1974. Optical properties of pure water and pure sea water, in: Jerlov, N. G. Nielsen, E.S. (Eds.), Optical Aspects of Oceanography, Academic Press, New York, pp. 1-24.

Morel, A., 1988. Optical modeling of the upper ocean in relation to its biogenous matter content (case 1 waters). J. Geophys. Res. 93, 10749-10768.

Morel, A., Maritorena, S., 2001. Bio-optical properties of oceanic water: A reappraisal. J. Geophys. Res. 106, 7163-7180.

Mouw, C. B., Yoder, J.A., 2005. Primary production calculations in the Mid-Atlantic Bight, including effects of phytoplankton community size structure. Limnol. Oceangr. 50, 1232-1243.

Mouw, C.B., Yoder, J.A., 2010. Optical determination of phytoplankton size composition from global SeaWiFS imagery. J. Geophys. Res., 115, C12018, doi:10.1029/2010JC006337.

O'Reilly, J. Maritorena, S., Mitchell, B.G., Siegel, D.A., Carder, K.L., Garver, S.A., Kahru, M., McClain, C., 1998. Ocean color chlorophyll algorithms for SeaWiFS. J. Geophys. Res. 103(C11), 24937-24953.

Orr, J.C, Fabry, V.J., Aumont, O., Bopp, L., Doney, S.C., Feely, R.A., Gnanadesikan, A., Gruber, N., Ishida, A., Joos, F., Key, R.M., Lindsay, K., Maier-Reimer, E., Matear, R., Monfray, P., Mouchet, A., Najjar, R.G., Plattner, G.-K., Rodgers, K.B., Sabine, C.L., Sarmiento, J.L., Schlitzer, R., Slater, R.D., Totterdell, I.J., Weirig, M.-F., Yamanaka, Y., Yool, A., 2005. Antropogenic ocean acidification over the twenty-first century and its impact on calcifying organisms. Nature. 437, 681-686, doi: 610.1038/nature04095.

Pope, R. M., Fry, E. S., 1997. Absorption spectrum (380-700 nm) of pure water. II. Integrating cavity measurements. Appl. Opt. 36, 8710-8723.

Rothstein, L.W., Cullen, J.J., Abbott, M.R., Chassignet, E.P., Denman, K.L., Doney, S.C., Ducklow, H.W., Fennel, K., Follows, M.J., Haidvogel, D., Hoffman, E.E., Karl, D.M., Kindle, J., Lima, I.D., Maltrud, M., McClain, C.R., McGillicuddy, D.J., Olascoaga, M.J., Spitz, Y., Wiggert, J., Yoder, J.A., 2006. Modeling Ocean Ecosystems: the PARADIGM program. Oceanography. 19, 23-51.

Siegel, D.A., S. Maritorena, N.B. Nelson, D.A. Hansell, M. Lorenzi-Kayser, 2002. Global distribution and dynamics of colored dissolved and detrital organic materials. J. Geophys. Res. 107, 3228, doi:10.1029/2001JC000965.

Smith, R., Gent, P., 2004. Ocean component of the Community Climate System model (CCSM2.0 and 3.0), Reference manual for the Parallel Ocean Program (POP).

Stramski, D., Reynolds, R., Kahru, M., Mitchell, B.G., 1999. Estimation of particulate organic carbon in the ocean from satellite remote sensing. Science. 285, 239-242.

Subramaniam, A., Carpenter, E. J., Falkowski, P.G., 1999a. Bio-optical properties of the marine diazotrophic cyanobacteria Trichodesmium spp. II. A reflectance model for remote sensing. Limnol. Oceangr. 44, 618-627.

Subramaniam, A., Carpenter, E. J., Karentz, D., Falkowski, P.G., 1999b. Bio-optical properties of the marine diazotrophic cyanobacteria Trichodesmium spp. I. Absorption and photosynthetic action spectra. Limnol. Oceangr. 44, 608-617.

Tjiputra, J. F., Polzin, D., Winguth, A. M. E., 2007. Assimilation of seasonal chlorophyll and nutrient data into an adjoint three-dimensional ocean carbon cycle model: Sensitivity analysis and ecosystem parameter optimization. Global Biogeochem. Cycles. 21, GB1001, doi:10.1029/2006GB002745.

Uitz, J., Claustre, H., Morel, A., Hooker, S.B., 2006. Verical distribution of phytoplankton communities in open ocean: an assessment based on surface chlorophyll. J. Geophys. Res. 111, C08005, 10.1029/2005JC003207.

Westberry, T. K., Siegel, D. A., Subramaniam, A., 2005. An improved bio-optical model for the remote sensing of Trichodesmium spp. blooms. J. Geophys. Res. 110, C06012, doi: 10.1029/2004JC002517.

Table 1. Summary of optical parameter notation

$a^*_{micro}(\lambda)$	chlorophyll-specific spectral absorption due to microphytoplankton ($m^2\ mg^{-1}$)
$a^*_{pico}(\lambda)$	chlorophyll-specific spectral absorption due to picophytoplankton ($m^2\ mg^{-1}$)
$a^*_{size}(\lambda)$	chlorophyll-specific spectral absorption of phytoplankton weighted by S_{fm} ($m^2\ mg^{-1}$)
$a^*_{tri}(\lambda)$	chlorophyll-specific spectral absorption due to *Trichodesmium* spp. ($m^2\ mg^{-1}$)
$a^*_{Ciotti\text{-}avg}(\lambda)$	chlorophyll-specific spectral absorption due to an average of the Ciotti pico-, ultra-, nano- and microplankton absorption spectra ($m^2\ mg^{-1}$)
$a^*_{cdm}(\lambda)$	weight-specific spectral absorption due to the combined effect of colored dissolved and detrital matter ($m^2\ mg^{-1}$)
$a_{size}(\lambda)$	spectral absorption due to phytoplankton weighted by S_{fm} (m^{-1})
$a_{tri}(\lambda)$	spectral absorption due to *Trichodesmium* spp. (m^{-1})
$a_w(\lambda)$	spectral absorption due to pure seawater (m^{-1})
$a_{cdm}(\lambda)$	spectral absorption due to the combined effect of colored dissolved and detrital matter (m^{-1})
$a(\lambda)$	total spectral absorption (m^{-1})
$b_{b\ size}(\lambda)$	spectral backscatter due to size dependent phytoplankton (m^{-1})
$b_{b\ tri}(\lambda)$	spectral backscatter due to *Trichodesmium* spp. (m^{-1})
$b^*_{b\ tri}(\lambda)$	weight-specific spectral backscatter due to *Trichodesmium* spp. ($m^2\ mg^{-1}$)
$b_{size}(\lambda)$	spectral scattering due to size dependent phytoplankton (m^{-1})
$b_{tri}(\lambda)$	spectral scattering due to *Trichodesmium* spp. (m^{-1})
$b_w(\lambda)$	spectral scattering due to seawater (m^{-1})
$b(\lambda)$	spectral total scattering (m^{-1})
S_f	percent picoplankton (%)
S_{fm}	percent microplankton (%)
$[Chl_{size}]$	phytoplankton size dependent chlorophyll concentration (mg m^{-3})
$[Chl_{micro}]$	microplankton chlorophyll concentration (mg m^{-3})
$[Chl_{small}]$	combined picoplankton and nanoplankton chlorophyll concentration (mg m^{-3})
$[Chl_{tri}]$	*Trichodesmium* spp. chlorophyll concentration (mg m^{-3})
λ,λ_0	wavelength, reference wavelength (443 nm) (nm)
S	slope of the spectral $a_{cdm}(\lambda)$ relationship (nm^{-1})
$Color_{cdm}$	colored fraction of the DOC pool (%)
[DOC]	dissolved organic carbon concentration (mg C m^{-3})
[CDM]	concentration of colored dissolved and detrital matter (mg m^{-3})
ν	exponent of the $b_{bsize}(\lambda)$ relationship that varies with $[Chl_{size}]$
B_{size}	backscattering ratio for size dependent phytoplankton (b_b/b, dimensionless)
B_{tri}	backscattering ratio for *Trichodesmium* spp. (b_b/b, dimensionless)
$R_{rs}(\lambda)$	spectral remote sensing reflectance (sr^{-1})
$\hat{R}_{rs}(\lambda)$	normalized remote sensing reflectance (dimensionless)
$\hat{R}_{rs}(\lambda)_{chl}$	normalized remote sensing reflectance for the constant chlorophyll scenario (case 1, dimensionless)
$\hat{R}_{rs}(\lambda)_{S_{fm}}$	normalized remote sensing reflectance for the constant size scenario (case 1, dimensionless)

$\hat{R}_{rs}(\lambda)_{dep-a}$	normalized remote sensing reflectance for the annual size-dependent scenario (case 1, dimensionless)
$\hat{R}_{rs}(\lambda)_{Ciotti-avg}$	normalized remote sensing reflectance for the Ciotti average size-independent absorption scenario (case 2, dimensionless)
$\hat{R}_{rs}(\lambda)_{dep-m}$	normalized size-independent remote sensing reflectance monthly size-dependent scenario (case 2, dimensionless)
$\hat{R}_{rs}(\lambda)_{indep-mean}$	normalized remote sensing reflectance for the model mean S_{fm} size-independent scenario (case 2, dimensionless)
K_d	diffuse attenuation coefficient (m^{-1})
z	depth (m)
PAR	photosynthetically active radiation (W m^{-2})

Table 2. 2004 annual summary of $\hat{R}_{rs}(443)$ and OC4 [Chl] global mean values for Ciotti-average size-independent, model mean size-independent and size-dependent chlorophyll-specific absorption scenarios from case study 2 and percent difference between the scenarios. 2004 global mean SeaWiFS $\hat{R}_{rs}(443)$ and OC4 [Chl] are presented for magnitude rather than validation comparison purposes.

	$\hat{R}_{rs}(443)$	**OC4 [Chl] (mg m^{-3})**
Ciotti-average Size-independent	4.61	0.174
Model Mean Size-independent	3.89	0.219
Size-dependent	4.00	0.216
Ciotti-average % difference	14.2%	-21.5%
Model Mean % difference	-2.79%	1.38%

Table 3. Correlation coefficient matrix of $\hat{R}_{rs}(443)_{Ciotti-avg}$, $\hat{R}_{rs}(443)_{dep-m}$, and percent difference between the scenarios with [Chl_{size}] and S_{fm}.

	[Chl_{size}]	**S_{fm}**
$\hat{R}_{rs}(443)_{Ciotti-avg}$	-0.89	0.50
$\hat{R}_{rs}(443)_{dep-m}$	-0.87	0.68
% difference	-0.43	0.91
[Chl_{size}]	-	-0.35
S_{fm}	-0.35	-

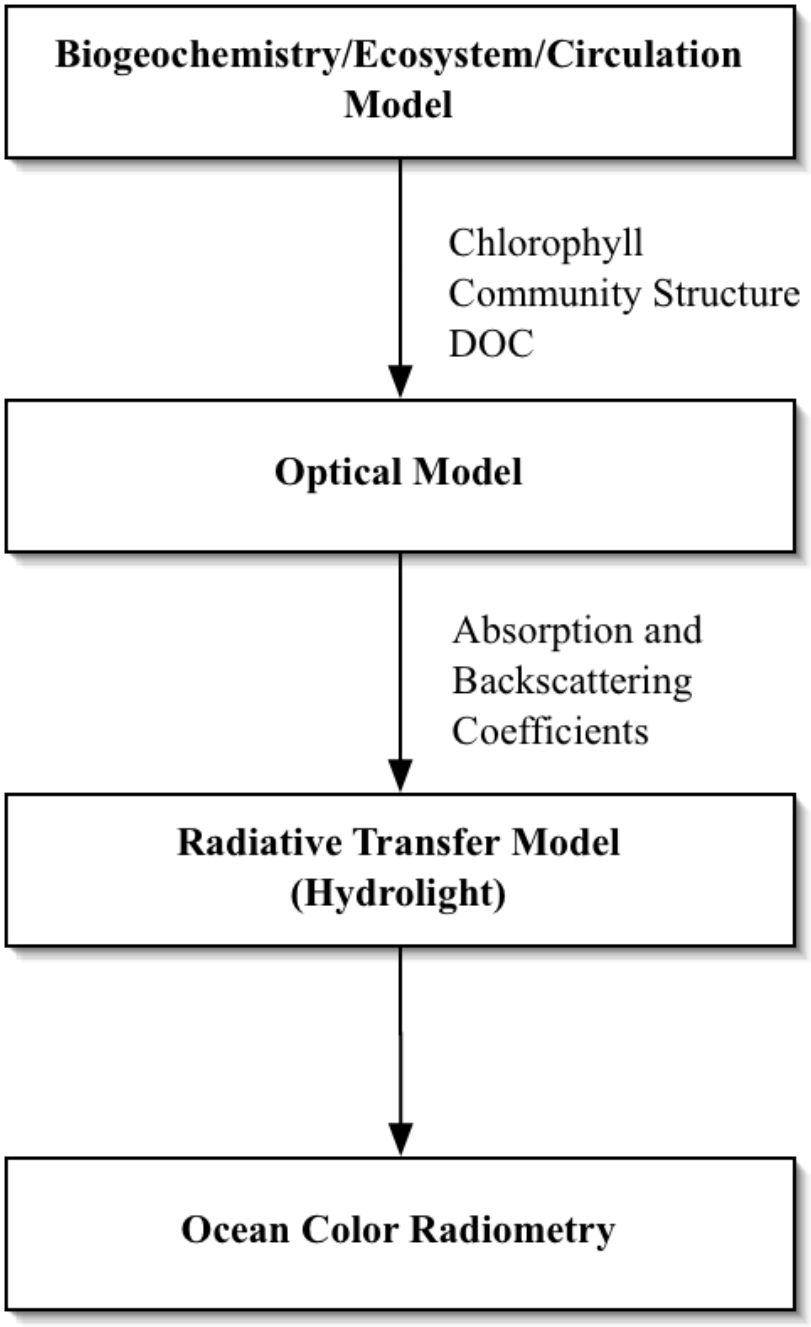

Figure 1. Schematic overview of the Community Climate System Model-3 coupled Biogeochemical Elemental Cycling model output linked in an offline diagnostic manner with the forward optical model.

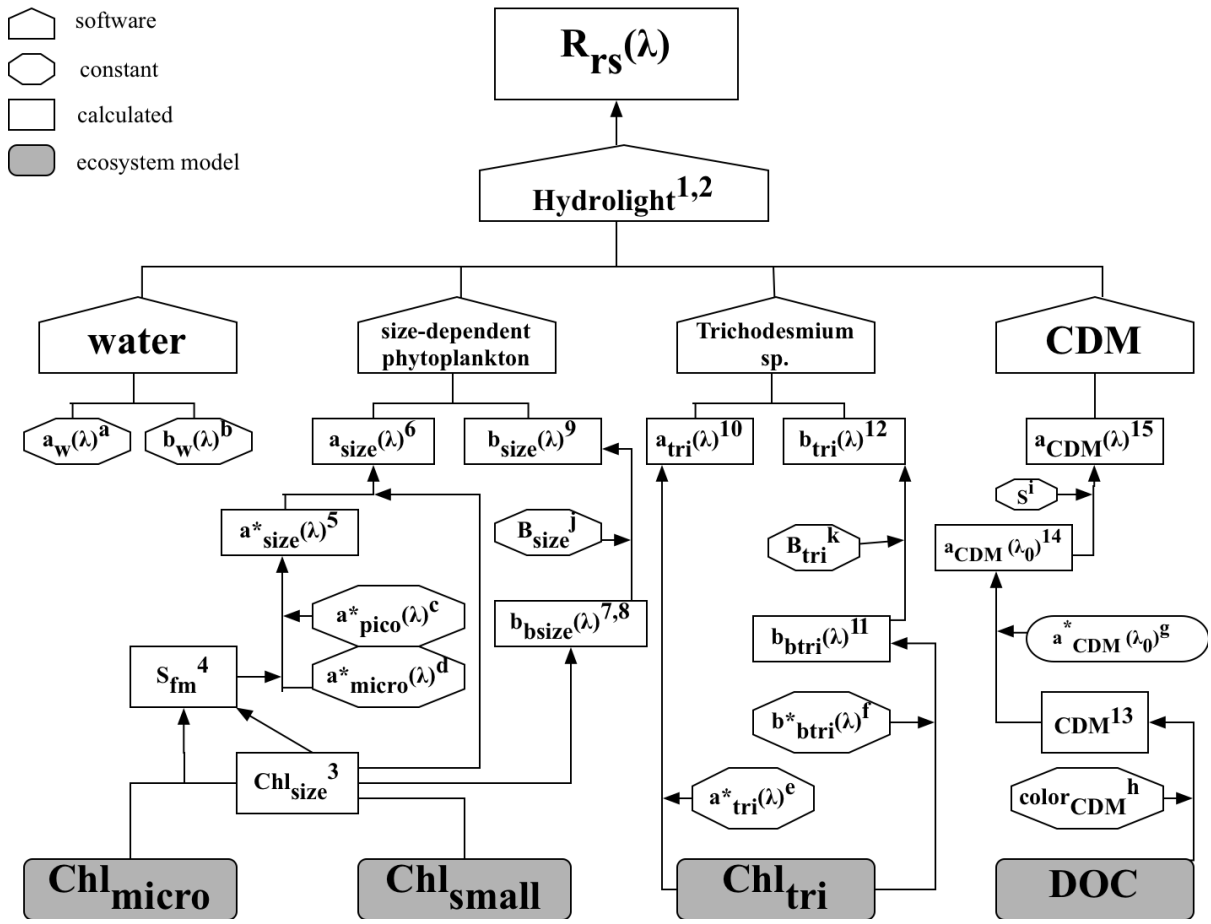

Figure 2. Schematic diagram and equations for the forward optical model. Superscript numbers next to each parameter refers to the equation numbers as listed in the text; superscript letters indicate reference for constant values ([a] $a_w(\lambda)$ (Pope and Fry, 1997),[b] $b_w(\lambda)$ (Morel, 1974), [c] $a^*_{pico}(\lambda)$ (Ciotti and Bricaud, 2006), [d] $a^*_{micro}(\lambda)$ (Ciotti et al., 2002), [e] $a^*_{tri}(\lambda)$ (Subramaniam et al., 1999b), [f] $b^*_{btri}(\lambda)$ (Subramaniam et al., 1999a), [g] $a^*_{CDM}(410) = 5.08$ m^2g^{-1} (Bissett et al., 1999a; Bissett et al., 2004), [h] $color_{CDM} = 3.23\%$ (Bissett et al., 1999a; Bissett et al., 2004), [i] $S = 0.015$ nm^{-1} (Barnard et al., 1998), [j] B_{size} (b_b/b) = 1% (Morel and Maritorena, 2001), [k] B_{size} (b_b/b) = 0.4% (Subramaniam et al., 1999a).

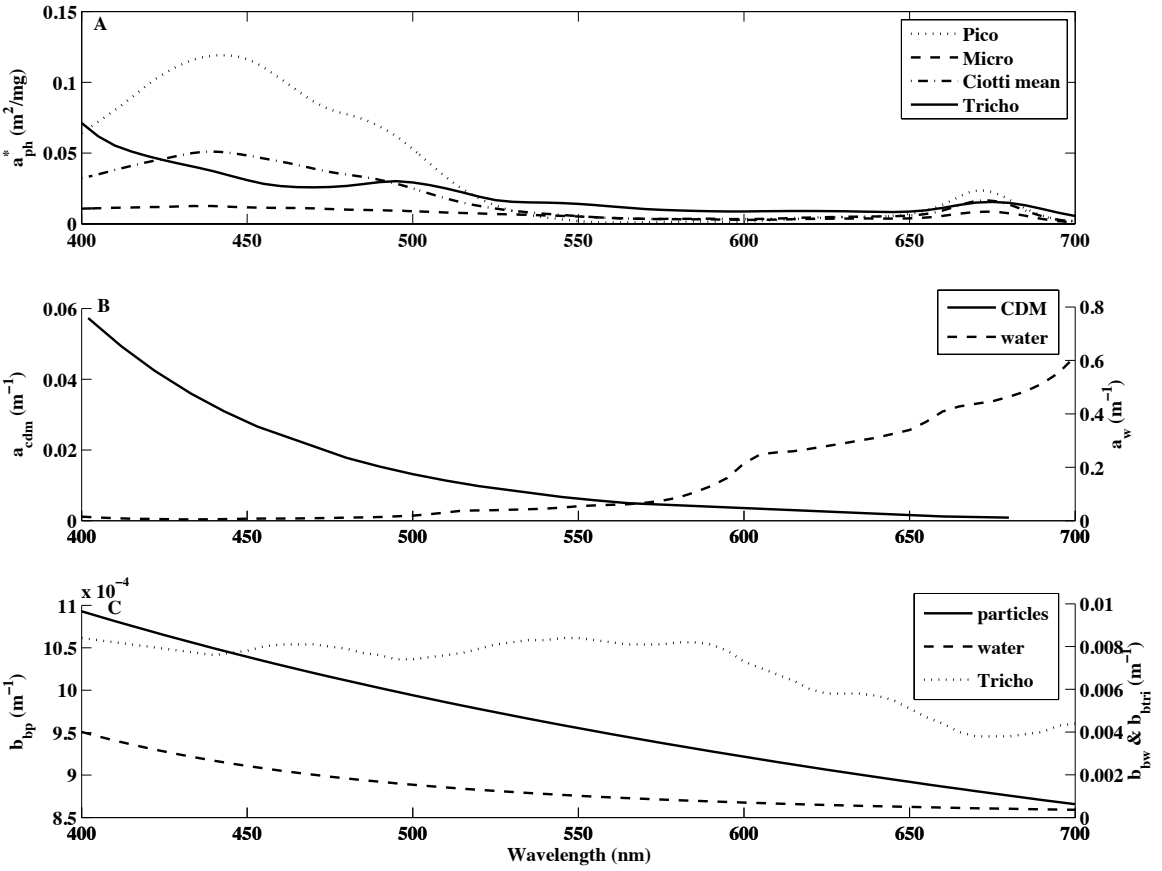

Figure 3. Absorption and backscattering spectra: A) spectral chlorophyll-specific phytoplankton absorption (a^*_{ph}) for pico- (Ciotti and Bricaud, 2006), microplankton (Ciotti et al., 2002), average of the micro-, ultra-, nano- (Ciotti et al., 2002) and picoplankton (Ciotti and Bricaud, 2006) size spectra, and *Trichodesmium* spp. (Subramaniam et al., 1999b; Westberry et al., 2005), B) spectral absorption coefficient for dissolved material (a_{CDM}) (Barnard et al., 1998; Bissett et al., 1999a; Bissett et al., 2004) and sea water (a_w) (Pope and Fry, 1997), C) spectral backscattering coefficient for particles which includes size dependent phytoplankton (b_{bp}) (Morel and Maritorena, 2001), water (b_{bw}) (Morel, 1974), and *Trichodesmium* spp. (b_{btri}) (Subramaniam et al., 1999a). a_{CDM}, b_{bp} and b_{btri} are concentration specific. In the examples here, 10 mg m^{-3}, 0.17 mg m^{-3}, and 1 mg m^{-3} were used for [CDM], [Chl_{size}] and [Chl_{tri}], respectively.

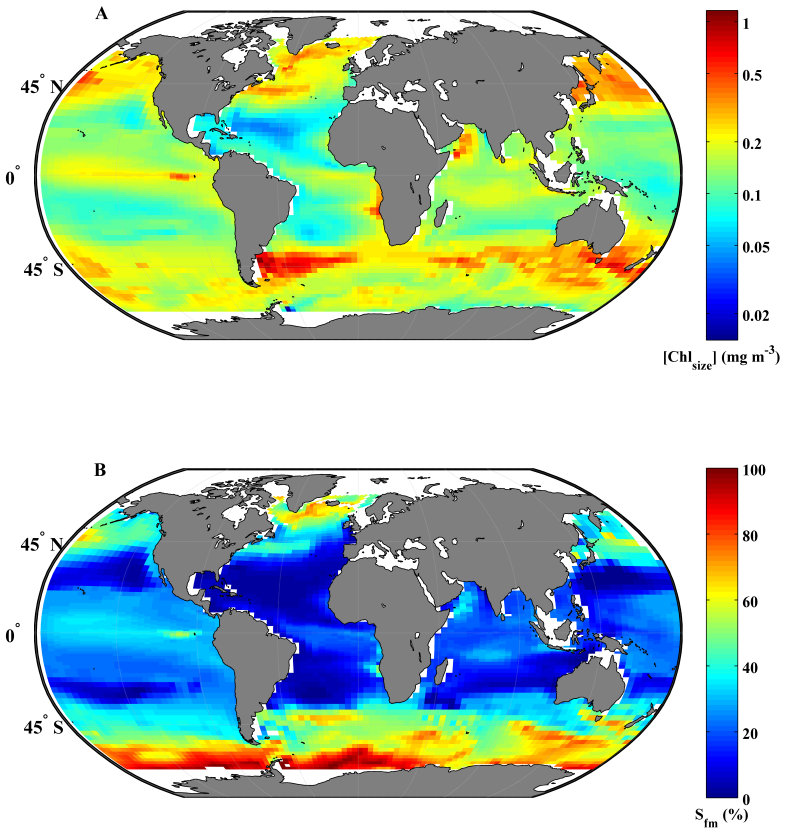

Figure 4. 2004 annual first optical depth mean CCSM-3 BEC model output for A) size dependent chlorophyll concentration ([Chl_{size}], mg m^{-3}) and, B) percentage of microplankton (S_{fm}, %). The color bar for panel A is non-linear to emphasize low values.

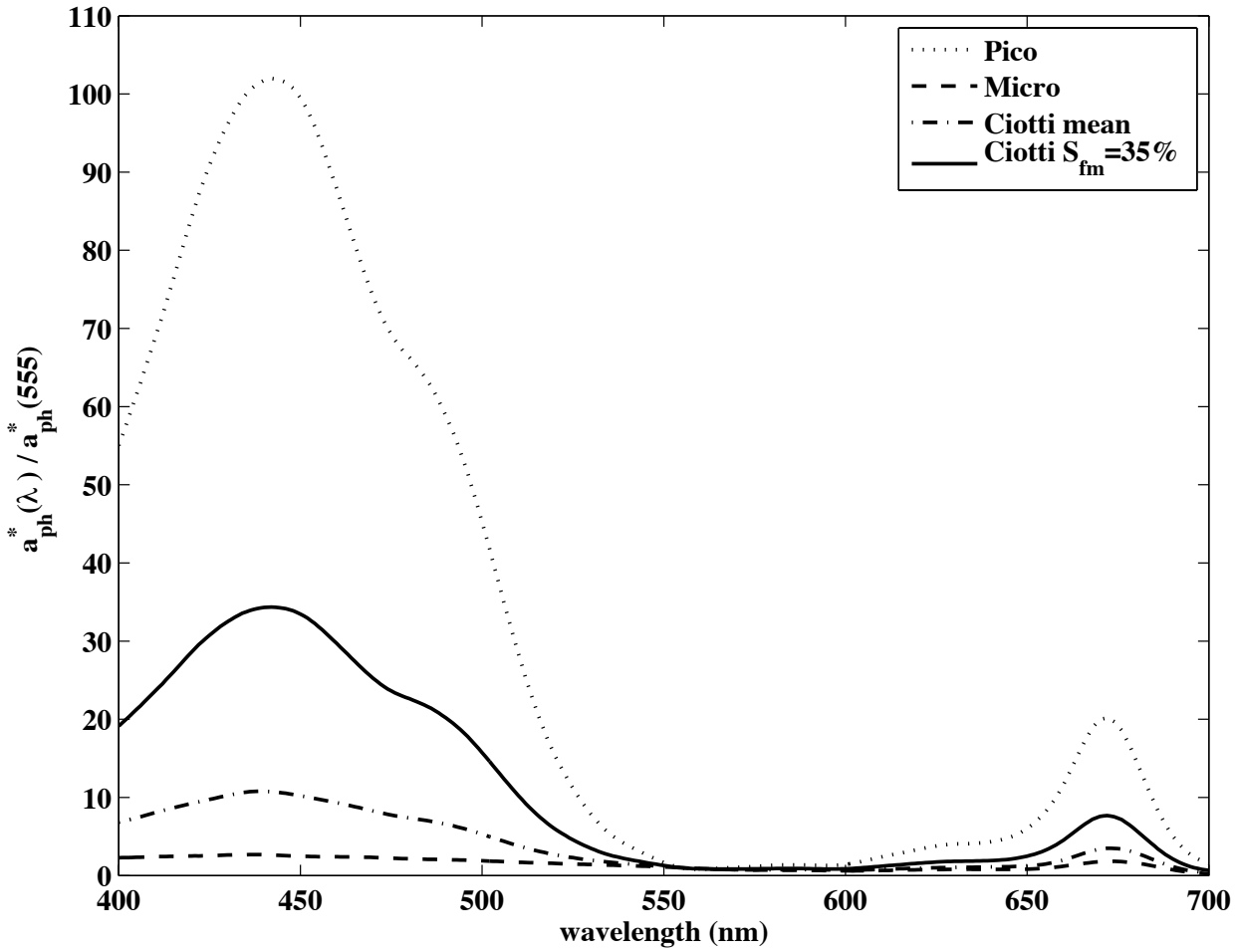

Figure 5. Chlorophyll-specific absorption spectra due to phytoplankton normalized to 555 nm. Microplankton (Ciotti et al., 2002), picoplankton (Ciotti and Bricaud 2006), the average of pico- (Ciotti and Bricaud, 2006), ultra-, nano- and microplankton (Ciotti et al. 2002), and the resulting spectra from the Ciotti et al. (2002) absorption spectral mixing model for the global mean percent microplankton from the CCSM-3 BEC model output (35%).

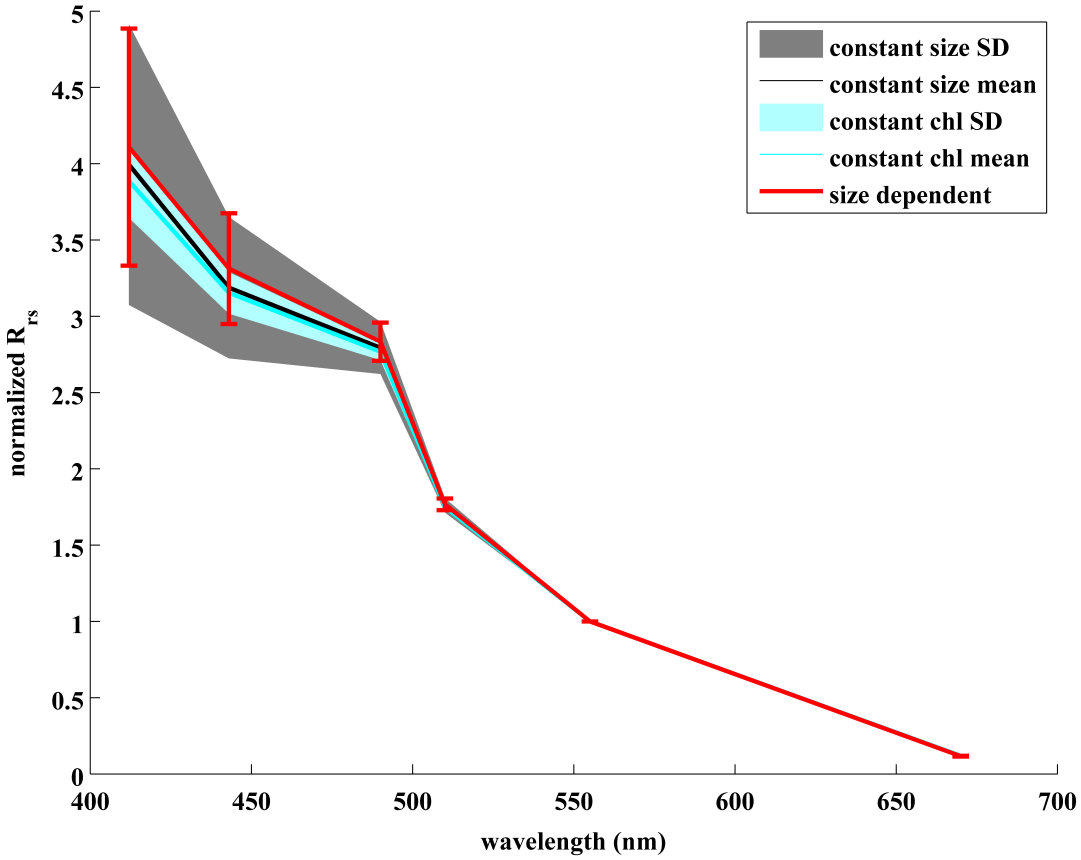

Figure 6. 2004 mean normalized remote sensing reflectance at 443 nm for the size dependent ($\hat{R}_{rs}(\lambda)_{dep-a}$, full variability, red line), constant size ($\hat{R}_{rs}(\lambda)_{S_{fm}}$, black), and constant chlorophyll ($\hat{R}_{rs}(\lambda)_{chl}$, blue) scenarios. The mean spectrum for each scenario is displayed as a line. Shading is used to indicate variability about the mean (one standard deviation) for the constant size (gray shading) and constant chlorophyll (blue shading) scenarios; the red error bars denote one standard deviation for the size dependent scenario. $\hat{R}_{rs}$ was computed only at specific wavelengths corresponding to the SeaWiFS bands.

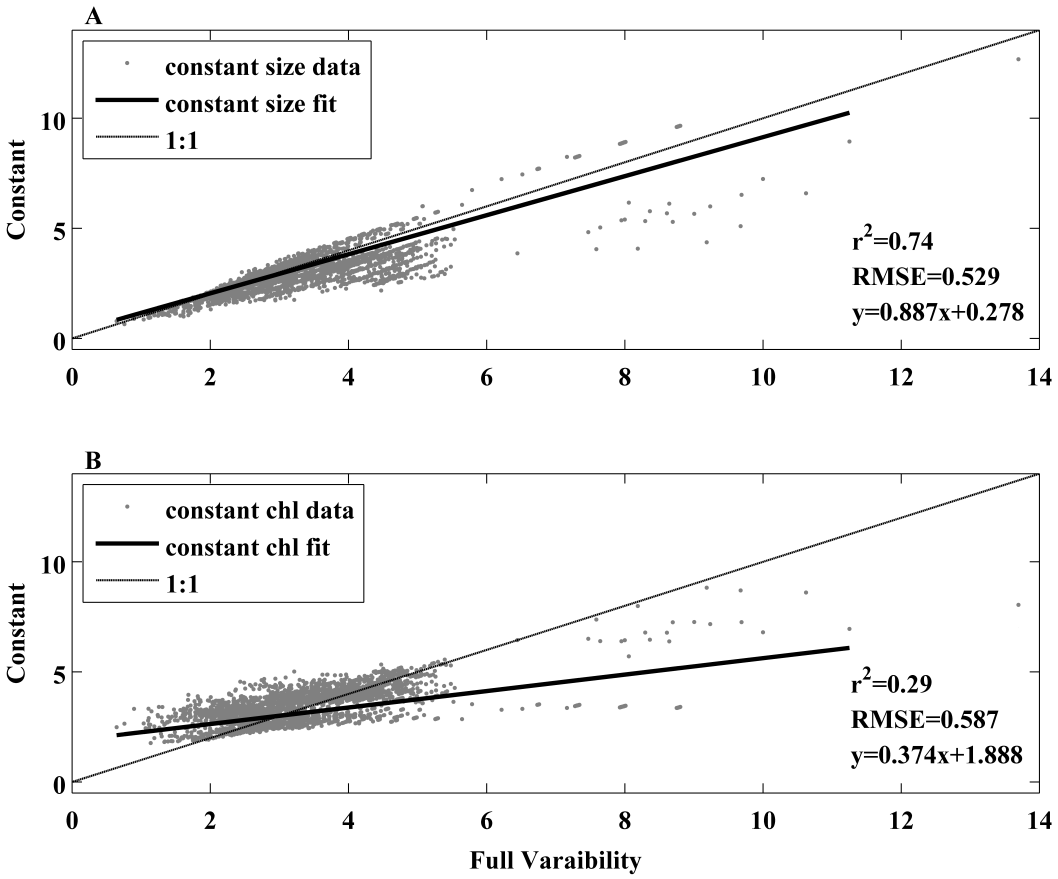

Figure 7. Scatter plots of 2004 mean normalized remote sensing reflectance at 443 nm ($\hat{R}_{rs}(443)$, dimensionless) comparing estimates of the size-dependent scenario (full variability in all parameters) with estimates when A) cell size and B) chlorophyll concentration are held constant. A linear regression was preformed for each case. The 1:1 line is plotted for comparison.

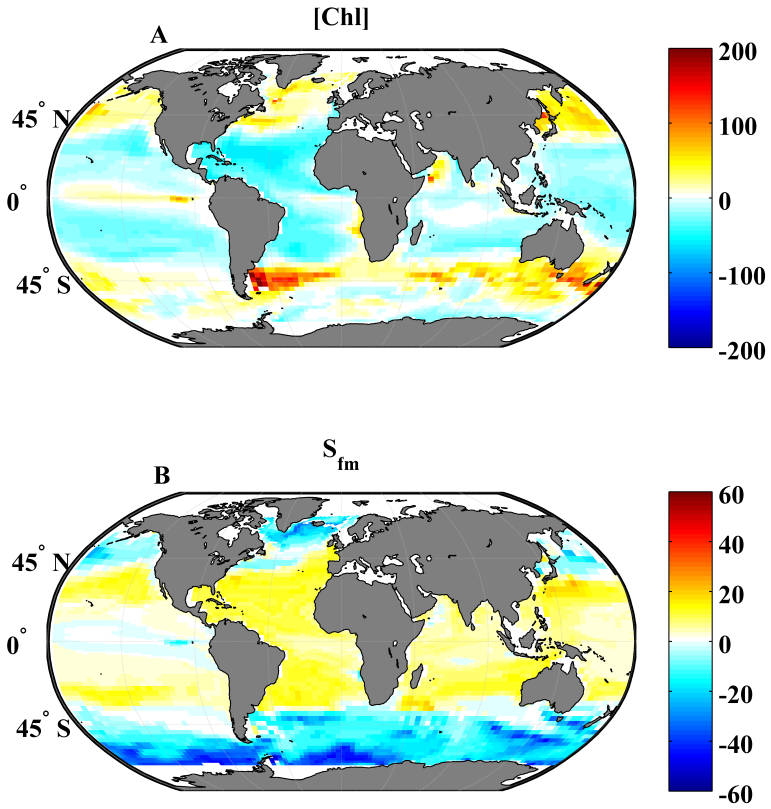

Figure 8. 2004 annual percent fractional error of normalized remote sensing reflectance at 443 nm for the A) constant chlorophyll concentration ($\hat{R}_{rs}(443)_{chl}$), and B) constant size scenarios ($\hat{R}_{rs}(443)_{S_{fm}}$). Percent fractional error was calculated as $\left[\frac{(\hat{R}_{rs}(443)_{chl} - \hat{R}_{rs}(443)_{dep-a})}{\hat{R}_{rs}(443)_{dep-a}}\right] \times 100$ and $\left[\frac{(\hat{R}_{rs}(443)_{S_{fm}} - \hat{R}_{rs}(443)_{dep-a})}{\hat{R}_{rs}(443)_{dep-a}}\right] \times 100$ respectively. Note the larger scale in the color bar of panel A) compared to panel B).

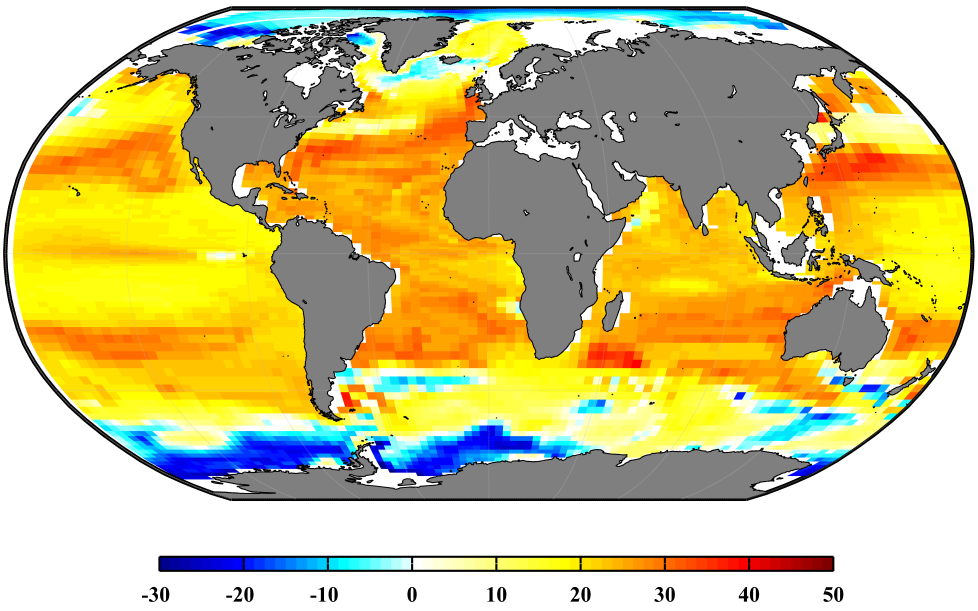

Figure 9. 2004 mean annual percent difference between normalized remote sensing reflectance at 443 nm size-independent ($\hat{R}_{rs}(443)_{Ciotti-avg}$) and size-dependent absorption ($\hat{R}_{rs}(443)_{dep-m}$) simulations.

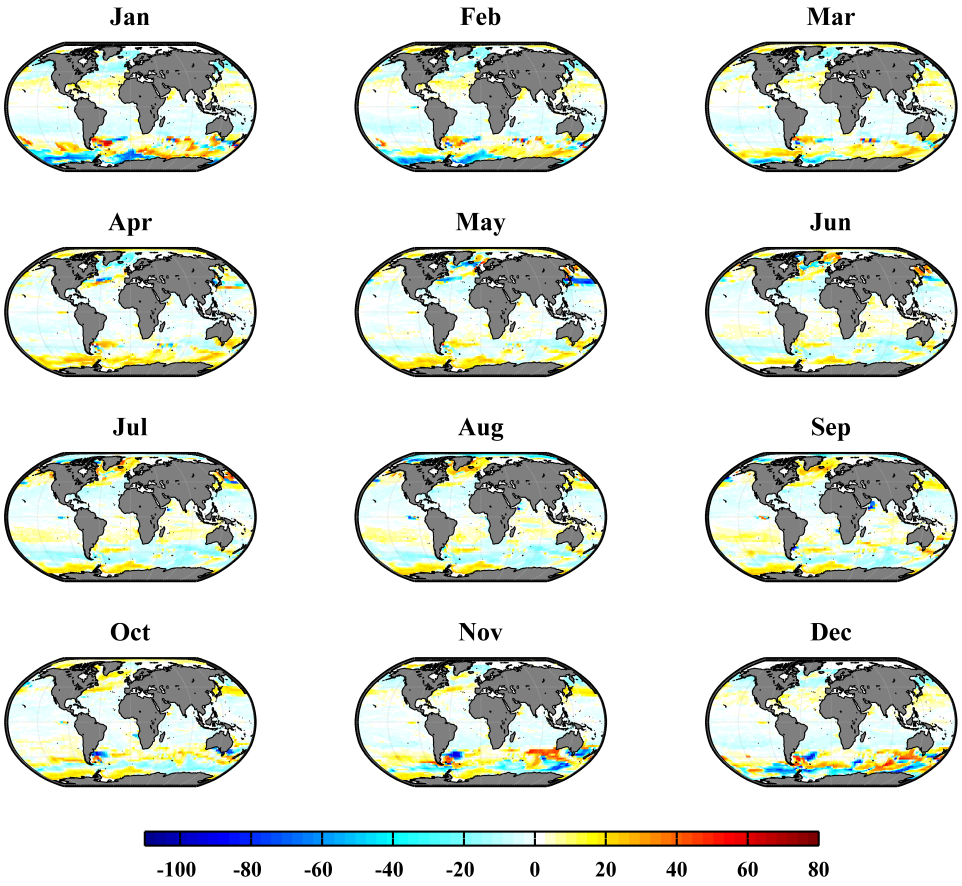

Figure 10. 2004 monthly $\hat{R}_{rs}(\lambda)$ percent difference between normalized remote sensing reflectance at 443 nm size-independent ($\hat{R}_{rs}(443)_{Ciotti-avg}$) and size-dependent absorption ($\hat{R}_{rs}(443)_{dep-m}$) simulations after the spatially varying annual mean percent difference was subtracted from each monthly grid cell.

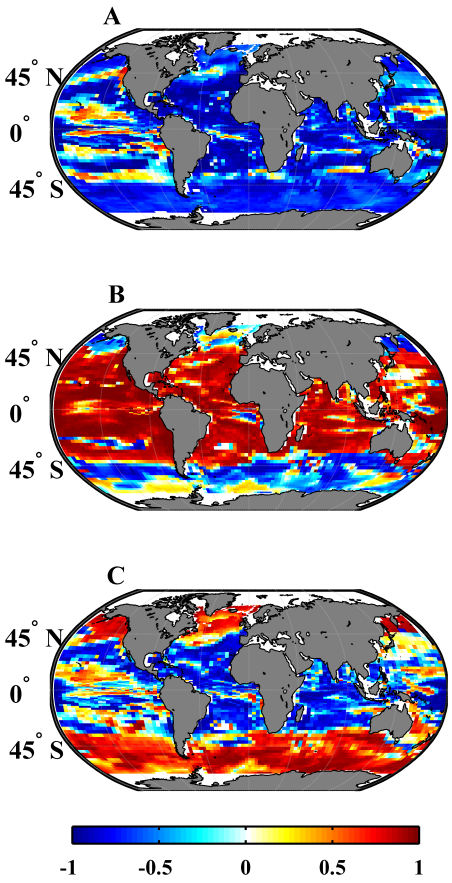

Figure 11. 2004 correlation coefficient (r^2) for the second case scenarios. Linear regression was performed at a given grid cell for the monthly CCSM-3 BEC output. The r^2 is mapped between A) $\hat{R}_{rs}(443)_{dep-m}$ and [Chl_{size}], B) [Chl_{size}] and S_{fm}, and C) $\hat{R}_{rs}(443)_{dep-m}$ and S_{fm}, respectively.

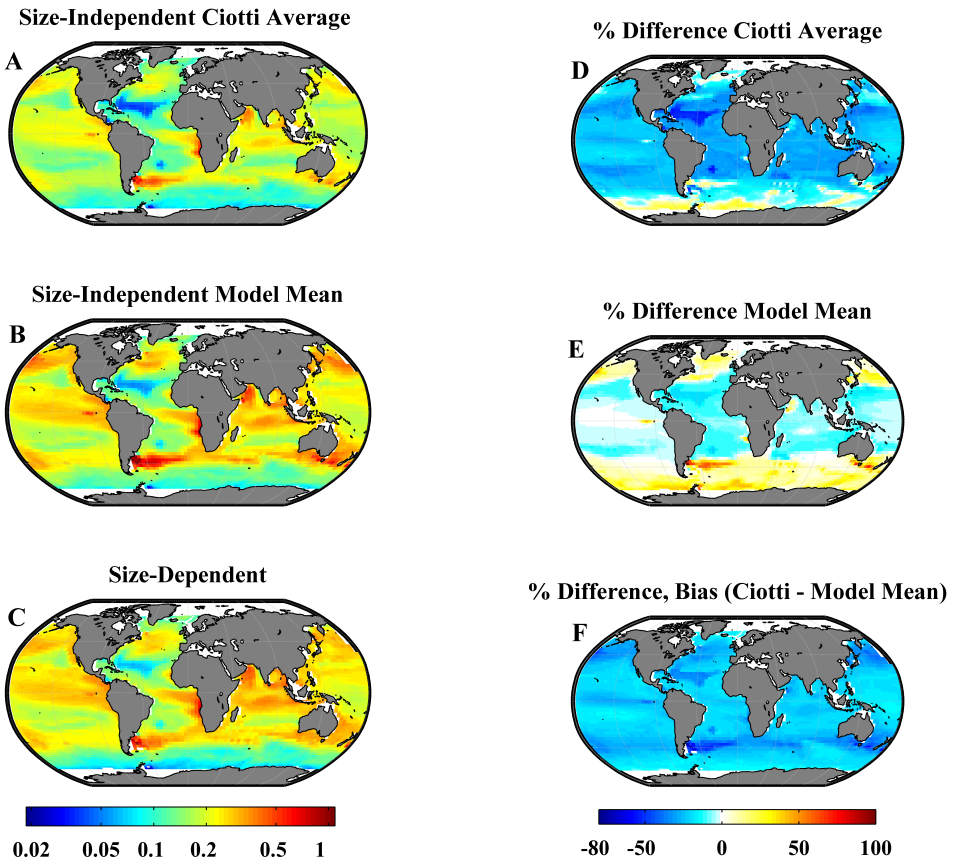

Figure 12. SeaWiFS standard band-ratio chlorophyll concentration (OC4 [Chl], mg m^{-3})) (O'Reilly et al., 1998) resulting from the spectral remote sensing reflectance values for the second case study of A) size-independent chlorophyll-specific absorption ($R_{rs}(\lambda)_{Ciotti-avg}$), B) size-independent model mean chlorophyll-specific absorption ($R_{rs}(\lambda)_{indep-mean}$, S_{fm} = 35%), C) size-dependent chlorophyll-specific absorption ($R_{rs}(\lambda)_{dep-m}$) scenarios, D) chlorophyll percent difference between $R_{rs}(\lambda)_{Ciotti-avg}$ and $R_{rs}(\lambda)_{dep-m}$, E) chlorophyll percent difference between $R_{rs}(\lambda)_{indep-mean}$ and $R_{rs}(\lambda)_{dep-m}$ and F) chlorophyll percent difference bias, calculated as the difference between the chlorophyll percent difference for $R_{rs}(\lambda)_{Ciotti-avg}$ and $R_{rs}(\lambda)_{indep-mean}$ (i.e. panels D-E).

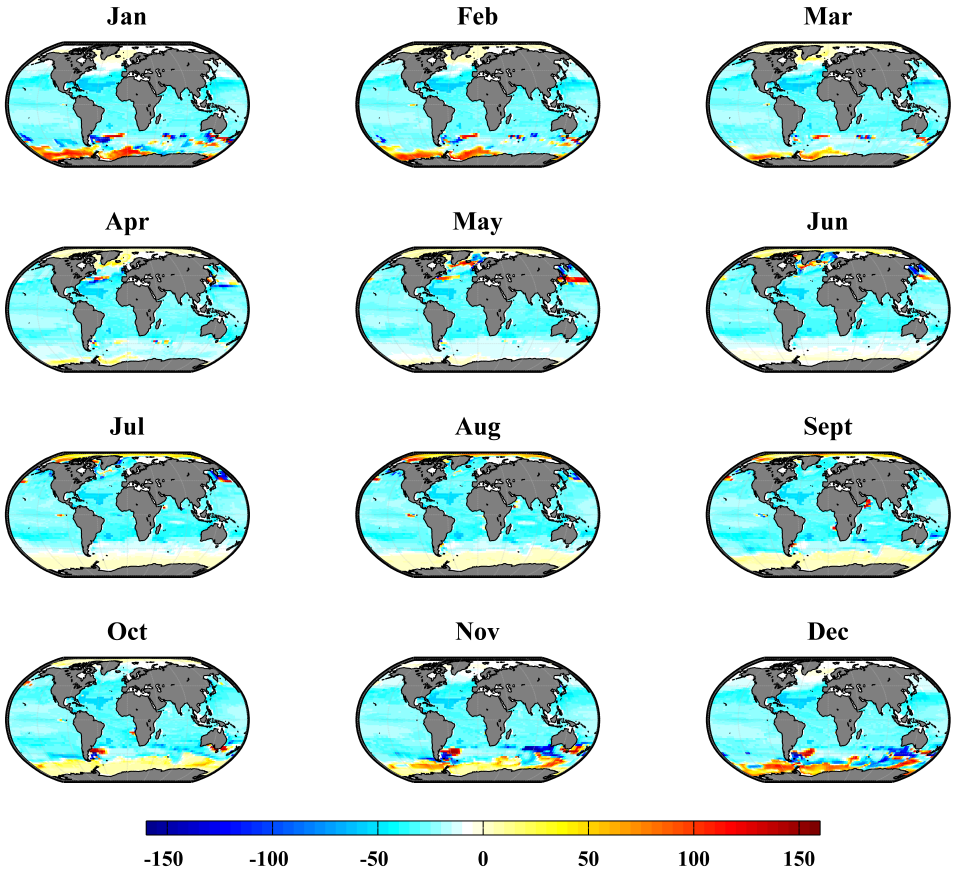

Figure 13. 2004 monthly percent difference for the SeaWiFS standard band-ratio chlorophyll concentration (OC4 [Chl], mg m^{-3}) calculated from the spectral remote sensing reflectance values for the size-independent absorption ($R_{rs}(\lambda)_{Ciotti-avg}$) and size-dependent absorption ($R_{rs}(\lambda)_{dep-m}$) scenarios.